

NAVAL POSTGRADUATE SCHOOL
Monterey, California

AD-A278 580



THESIS

SIGNAL PROCESSING FOR THE
1992 BARENTS SEA
TOMOGRAPHY EXPERIMENT

by

Philip G. McLaughlin

December, 1993

Thesis Advisors:

James H. Miller
Ching-Sang Chiu

Approved for public release; distribution is unlimited.

*Original contains color
plates: All DTIC reproductions
will be in black and
white*

94-12646

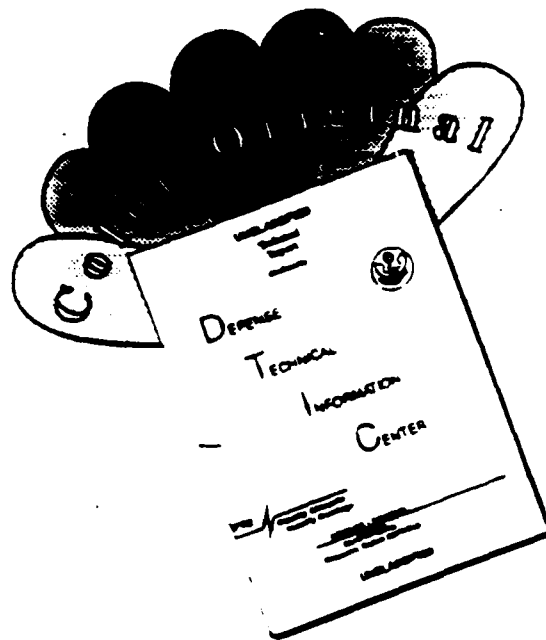


DTIC QUALITY INSPECTED 3

94 4 25 058

DTIC
ELECTE
APR 26 1994
S G D

DISCLAIMER NOTICE



THIS DOCUMENT IS BEST QUALITY AVAILABLE. THE COPY FURNISHED TO DTIC CONTAINED A SIGNIFICANT NUMBER OF COLOR PAGES WHICH DO NOT REPRODUCE LEGIBLY ON BLACK AND WHITE MICROFICHE.

REPORT DOCUMENTATION PAGEForm Approved
OMB No. 0704-0188

Public reporting burden for this collection of information is estimated to average 1 hour per response, including the time for reviewing instructions, searching existing data sources, gathering and maintaining the data needed, and completing and reviewing the collection of information. Send comments regarding this burden estimate or any other aspect of this collection of information, including suggestions for reducing this burden, to Washington Headquarters Services, Directorate for Information Operations and Reports, 1215 Jefferson Davis Highway, Suite 1204, Arlington, VA 22202-4302, and to the Office of Management and Budget, Paperwork Reduction Project (0704-0188), Washington, DC 20503.

1. AGENCY USE ONLY (Leave blank)**2. REPORT DATE**

December 1993

3. REPORT TYPE AND DATES COVERED

Master's Thesis

4. TITLE AND SUBTITLESIGNAL PROCESSING FOR THE 1992 BARENTS SEA TOMOGRAPHY
EXPERIMENT**5. FUNDING NUMBERS****6. AUTHOR(S)**

McLaughlin, Philip G.

7. PERFORMING ORGANIZATION NAME(S) AND ADDRESS(ES)Naval Postgraduate School
Monterey, CA 93943-5000**8. PERFORMING ORGANIZATION
REPORT NUMBER****9. SPONSORING/MONITORING AGENCY NAME(S) AND ADDRESS(ES)**Naval Postgraduate School
Monterey, CA 93943-5000**10. SPONSORING/MONITORING
AGENCY REPORT NUMBER****11. SUPPLEMENTARY NOTES****12a. DISTRIBUTION/AVAILABILITY STATEMENT**

UNLIMITED DISTRIBUTION

12b. DISTRIBUTION CODE

A

13. ABSTRACT (Maximum 200 words)

In August 1992, an acoustic tomography experiment was conducted in the Barents Sea. The objective of this thesis is the development of space-time signal processing algorithms to extract the arrival times of rays and modes for that experiment. The temporal signal processing involves pulse compression of the phase-encoded signal. Spatial signal processing consists of plane wave and modal beamforming on data from a 16 element vertical line array. After signal processing an arrival detection, identification, and tracking algorithm is used to obtain travel time and travel time error estimates. After development and testing of these algorithms, 13 hours of acoustic data was processed for rays and eight hours of data was processed for modes. The resultant travel time information is then available for inversion to sound speed maps.

DTIC QUALITY INSPECTION 3

14. SUBJECT TERMS**15. NUMBER OF PAGES**

71

16. PRICE CODE**17. SECURITY CLASSIFICATION
OF REPORT**

UNCLASSIFIED

**18. SECURITY CLASSIFICATION
OF THIS PAGE**

UNCLASSIFIED

**19. SECURITY CLASSIFICATION
OF ABSTRACT**

UNCLASSIFIED

20. LIMITATION OF ABSTRACT

UNLIMITED

Approved for public release; distribution is unlimited.

Signal Processing for the
1992 Barents Sea
Tomography Experiment

by

Philip G. McLaughlin
Lieutenant, United States Navy
B.S.E.E., United States Naval Academy

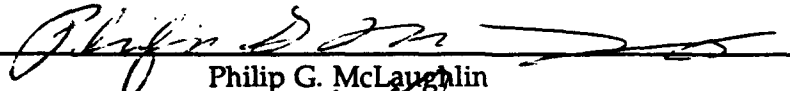
Submitted in partial fulfillment
of the requirements for the degrees of

MASTER OF SCIENCE IN ENGINEERING ACOUSTICS
and
MASTER OF SCIENCE IN ELECTRICAL ENGINEERING

from the

NAVAL POSTGRADUATE SCHOOL
December 1993

Author:

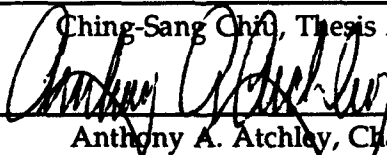

Philip G. McLaughlin

Approved by:


James H. Miller, Thesis Advisor



Ching-Sang Chiu, Thesis Advisor



Anthony A. Atchley, Chairman

Engineering Acoustics Academic Committee



Michael A. Morgan, Chairman

Department of Electrical and Computer Engineering

ABSTRACT

In August 1992, an acoustic tomography experiment was conducted in the Barents Sea. The objective of this thesis is the development of space-time signal processing algorithms to extract the arrival times of rays and modes for that experiment. The temporal signal processing involves pulse compression of the phase-encoded signal. Spatial signal processing consists of plane wave and modal beamforming on data from a 16 element vertical line array. After signal processing an arrival detection, identification, and tracking algorithm is used to obtain travel time and travel time error estimates. After development and testing of these algorithms, 13 hours of acoustic data was processed for rays and eight hours of data was processed for modes. The resultant travel time information is then available for inversion to sound speed maps.

Accession For	
NTIS CRA&I	<input checked="" type="checkbox"/>
DTIC TAB	<input type="checkbox"/>
Unannounced	<input type="checkbox"/>
Justification	
By	
Distribution /	
Availability Codes	
Dist	Avail and/or Special
A-1	

TABLE OF CONTENTS

I. INTRODUCTION	1
A. ACOUSTIC TOMOGRAPHY IN THE LITTORAL REGION	1
B. MOVING TOMOGRAPHY FROM DEEP TO SHALLOW WATER .	1
C. OVERVIEW OF THESIS	3
II. BARENTS SEA EXPERIMENT	7
A. EXPERIMENT OBJECTIVES	7
B. EXPERIMENT LOCATION	8
C. EQUIPMENT DESCRIPTION	12
III. ACOUSTIC TOMOGRAPHY THEORY	18
A. TOMOGRAPHY PROBLEM OVERVIEW	18
B. FORWARD PROBLEM	21
1. Plane Wave Propagation	21
2. Modal Propagation	22
C. SPACE-TIME SIGNAL PROCESSING	23
1. Temporal Signal Processing	23
2. Spatial Signal Processing	29

a. Plane Wave Beamforming	29
b. Mode Beamforming	31
IV. PERFORMANCE PREDICTIONS	37
A. PLANE WAVE PREDICTIONS	37
B. MODAL BEAMFORMER PREDICTIONS	44
V. RESULTS	49
A. PLANE WAVE	49
B. MODAL BEAMFORMING RESULTS	55
VI. SUMMARY AND FUTURE WORK	58
A. SIGNAL PROCESSING SUMMARY	58
B. FUTURE WORK	59
C. RECOMMENDATIONS	60
REFERENCES	61
INITIAL DISTRIBUTION LIST	63

ACKNOWLEDGEMENTS

There is a long list of people who have helped me throughout my research. Jim Miller and Ching-Sang Chiu certainly top the list. Their dedication, enthusiasm, and caring made work fun. To all the guys in the group, Jim Kresge, Chuck (Muggs) Muggleworth, and John Mykyta, thanks for listening and all the insightful recommendations you gave. Thanks to all the people I didn't get to know but helped in so many ways, Glenn Omans, Rost Parsons, Dr. Jim Lynch, Keith Von der Heydt, Dr. Robert Bourke, and the crew of the USS Bartlett. To the computer in tennis shoes (Stefan Hudson), thanks for keeping those babies (computers) purring. To all the acoustics guys in the physics department, Dr. Anthony Atchley, Dr. Oscar Wilson, Dr. Steve Baker, and Dr. Steve Garrett, thanks for all the lessons. To my family, Kara, Philip, and Kevin, thanks for giving me the freedom to do the work. Many thanks go to my parents, my father for inspiring me and my mother for being a great mom. A very special thank you goes to Chris Miller for all the help and friendship. I wish the greatest success for Chris in the future. The list is long so anyone inadvertently left off is unintentional.

I. INTRODUCTION

A. ACOUSTIC TOMOGRAPHY IN THE LITTORAL REGION

Future conflicts will require naval forces to operate in coastal regions [Ref. 1]. In order to achieve battle space dominance in these regions, the subsurface environment must be secured first. Securing the subsurface environment will require success in the prosecution of diesel submarines and in the hunting of mines. A key to success will be a detailed knowledge of ocean acoustic propagation. Traditional methods of obtaining the necessary environmental information will not provide the spatial resolution needed in a tactical time frame. Traditional methods can not provide sonar performance prediction of sufficient quality. Acoustic tomography provides a method to obtain the environmental information needed to determine and/or predict acoustic propagation with the necessary spatial resolution in a tactical time frame for the shallow water environment. Timely high resolution sound speed maps will be needed to achieve battle space dominance in littoral regions.

B. MOVING TOMOGRAPHY FROM DEEP TO SHALLOW WATER

Ocean acoustic tomography was originally proposed by Munk and Wunsch in 1977. In 1979, they presented methods for inverting the data to estimate the sound speed field [Ref. 2]. The procedure is similar to that used in medical x-ray tomography where the measuring signal travels in a straight line from source to receiver. Ocean acoustic

tomography relies on acoustic energy traveling over many paths with different travel times.

The word tomography is derived from two Greek roots meaning "to slice" and "to look at". Acoustic tomography is then looking at a slice of the ocean with acoustics. Sound speed is a function of salinity, pressure, and temperature. As acoustic energy travels along different paths, its speed depends upon these physical quantities. Travel time along these paths can be used to find a spatial sound speed map of the ocean. The knowledge of how sound speed affects travel time is known as the *forward problem*. The process of estimating sound speed from the travel time is known as the inverse problem or *inversion* [Ref. 2].

Tomography has been successfully used in deep water using receivers consisting of a single hydrophone or very simple arrays. Deep water tomography has been used to map regions of the deep ocean over ranges of 300 to 1000 km. This long travel distance provides sufficient separation in time for multipath arrival identification. Ray models are able to accurately describe much of the propagation. In shallow water, the acoustic propagation becomes more complex making the forward and inverse problems more difficult. Surface and bottom interactions occur frequently and multipath arrival identification and time estimation is made difficult by the lack of temporal separation. To identify these multipath arrivals, a vertical array can be used to provide temporal and spatial information on these arrivals. A vertical array can also be used as a spatial filter to beamform for the acoustic normal modes [Ref. 3, 4]. Thus a modal model can be used for propagation and inversion in addition to the ray model.

The primary advantage of acoustic tomography is its ability to sample an ocean volume quickly, i.e., at the speed of sound. For a typical shallow water survey, it may take many hours with traditional oceanographic sampling techniques to determine a sound speed field. Once the acoustic tomography source and receiver are in place, sound energy takes seconds to travel from the source to the vertical array. A sound speed field can be calculated as often as desired subject to the battery limitations of the sources and receivers. Tomography provides a unique method to view the interior of the ocean and its variability. Satellite remote sensing systems may be complimentary to tomography by providing information on features visible at the surface where resolution of the tomography maps may be poor. In addition, both tomography and satellite remote sensing data can be assimilated into an ocean model potentially providing very high resolution maps of a coastal ocean volume [Ref. 3].

C. OVERVIEW OF THESIS

The tomography problem is summarized in Figure 1.1. As Figure 1.1 shows, imaging the ocean sound speed variability with acoustic tomography requires a number of steps. The process starts with the development of a background environmental model. This model determines the path of acoustic propagation for the source to a receiver. The environmental model can be initialized with either historical data or in situ data obtained through traditional oceanography techniques. The acoustic data consists of a phase encoded sequence and timing information. Space-time signal processing is conducted to demodulate and decode the acoustic signal and provide spatial information for arrival

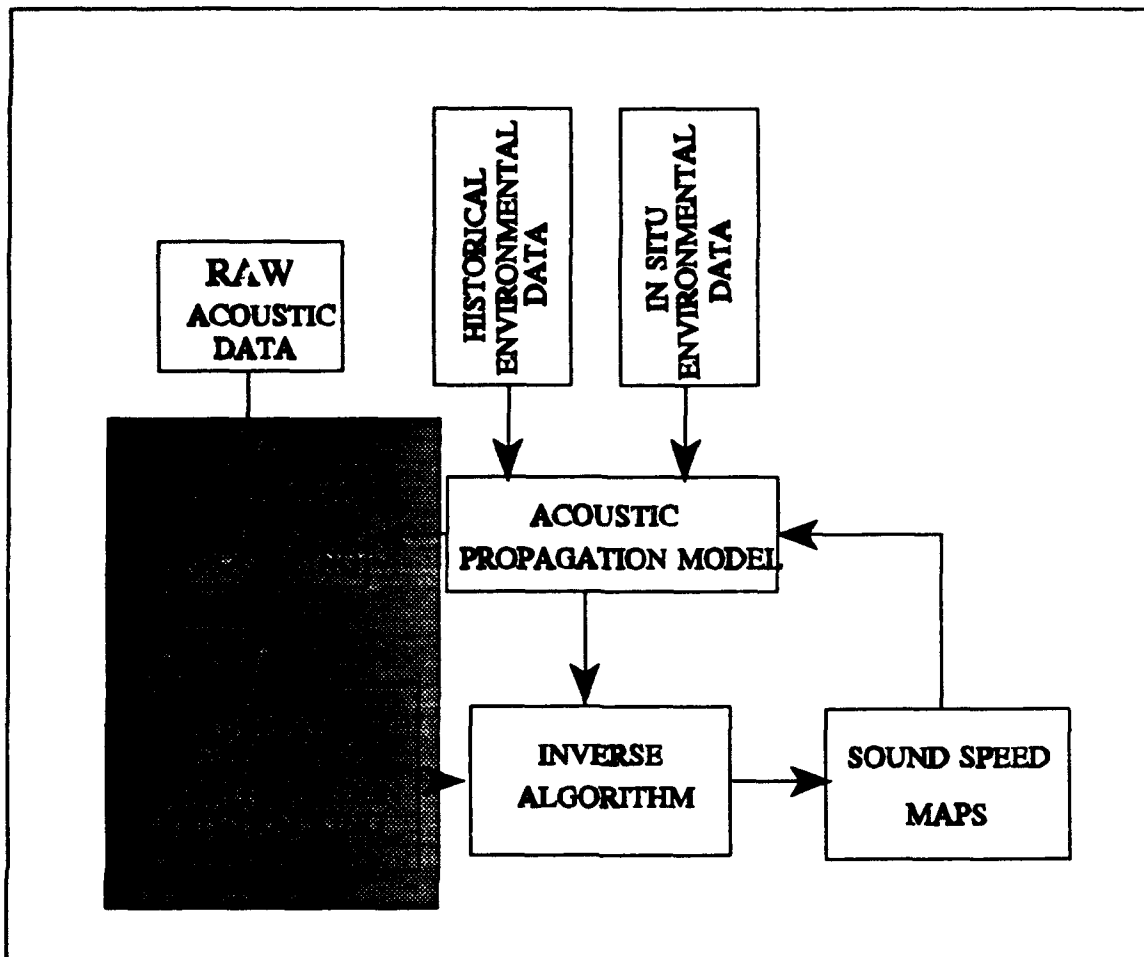


Figure 1.1: Acoustic tomography problem summary. This thesis contribution is indicated by region in gray.

identification. The environmental model influences the signal processing through beamforming and the expected arrival times. The array weights needed for a spatial matched filter for modal beamforming are provided by the environmental model. Arrival detection is performed in a temporal window around the expected arrival time provided by the environmental model. The difference between the actual arrival times as determined by the signal processing and arrival detection, and the expected arrival times is the information used by the inverse algorithm to determine the sound speed map. This

sound speed map may be used to improve the environmental model and an iterative solution may be determined.

The objectives of this thesis are to:

1. Develop space-time signal processing algorithms.
2. Develop arrival detection, identification, and tracking algorithms.
3. Assess beamformer performance.
4. Process 13 hours of acoustic data from the 1992 Barents Sea Polar Front Experiment.

The contribution of this thesis to the tomography problem is shown as the shaded region in Figure 1.1. The signal processing included plane wave beamforming, modal beamforming, and decoding of the signal. After the signal processing was complete, peak detection and travel time estimation were performed. All signal processing and peak detection algorithms were written in MATLAB™. MATLAB™ is a software package from the MathWorks Company.

A description of the 1992 Barents Sea Polar Front Experiment is contained in Chapter II. The description includes the physical setup of the experiment and its goals. A general description of the oceanography is included for completeness.

Chapter III summarizes the basic acoustic tomography theory. The discussion begins with propagation theory including both ray and mode theory. The discussion then shifts to the acoustic signal. Reasons for transmitting a maximal length phase encoded signal is discussed along with a description of these signals. Beamforming theory is

covered including both plane wave and modal. Finally all these pieces are tied together with a discussion of the tomographic inverse problem.

Predictions for beamformer performance are covered in Chapter IV. These predictions included array beampatterns and expected output. Synthetic data is used for later comparisons with experimental data.

Chapter V discusses results from the processing of data. These results are compared with the predictions of Chapter IV. Results from inversions of data are included.

Chapter VI summarizes the work completed and discusses lessons learned. Future work recommendations are given.

II. BARENTS SEA EXPERIMENT

A. EXPERIMENT OBJECTIVES

The Barents Sea Polar Front Experiment (BSPFEX) was conducted in August of 1992. The experiment was a joint effort between the Naval Postgraduate School (NPS), Woods Hole Oceanographic Institution (WHOI), and the Science Applications International Corporation (SAIC). The principal investigators for the experiment are Professors Ching-Sang Chiu, James H. Miller, and Robert Bourke from NPS, Dr. James F. Lynch from WHOI, and Dr. Robin Muench from SAIC. The principal engineers for the development and deployment vertical hydrophone array system were Mr. Keith Von der Heydt and Mr. John Kemp from WHOI. The objectives of the experiment as outlined by the Barents Sea Polar Front Group [Ref. 5] were:

1. Provide a detailed physical description of the polar front.
2. Enhance the understanding of dynamics of the front, including frontogenesis and its influence on regional oceanographic processes.
3. Assess the ability of acoustic tomography to define frontal and associated mesoscale features.
4. Provide improved documentation of shallow water acoustic propagation in this region and the effect of the environment on acoustic Anti-Submarine Warfare (ASW) operations.

B. EXPERIMENT LOCATION

The experiment was performed in the Barents Sea within a 80 x 90 km rectangle centered 100 km east of Bear Island as shown in Figure 2.1. The Barents Sea is bordered to the north by Spitzbergen and Franz Joseph Land, to the south by Scandinavia and Russia, to the east by Novaya Zemlya, and is open to the west. The experiment used both acoustic tomography and traditional oceanographic techniques to study the Barents Sea Polar Front [Ref. 6].

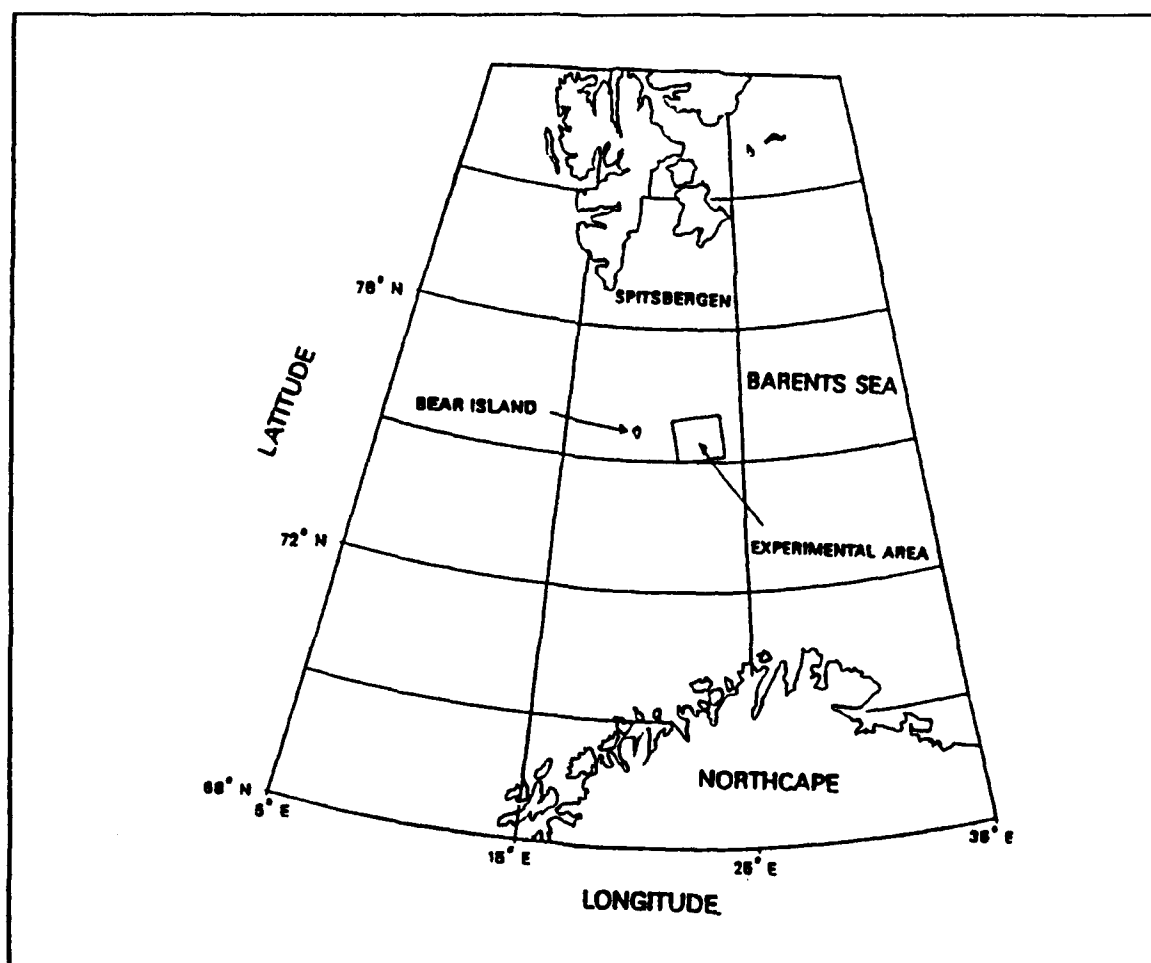


Figure 2.1: Experiment location.

The Barents Sea Polar Front is a stable feature which is caused by currents in the region [Ref 7]. These currents transport relatively cold fresh Arctic water and warm salty Atlantic waters to converge at the Barents Sea Polar Front. The characteristics of the different water masses are given in Table I and are shown in Figure 2.2. Figure 2.2 depicts Loeng's [Ref 8] model of the region. The abbreviations are: Arctic Water (AW), North Atlantic Water (NAW), Svalbard Bank Water (SBW), Barents Sea Water (BSW), and Bottom Water (BW). The experiment location is indicated by a rectangle in Figure 2.2.

Table I: Barents Sea Water Masses [Ref. 6]

Major Types	T (°C)	Salinity (psu)
Arctic Water (AW)	< .5	34.2 - 34.0
North Atlantic Water (NAW)	-.5 to 2.0	34.8 - 35.0

Local Variants	T (°C)	Salinity (psu)
Svalbard Bank Water (SBW)	1.0 to 3.0	< 34.4
Bottom Water (BW)	< -1.5	> 35.0
Barents Sea Water (BSW)	-1.5 to 2.0	34.7 - 35.0
Polar Front Water (PW)	-0.5 to 2.0	34.8 - 35.0

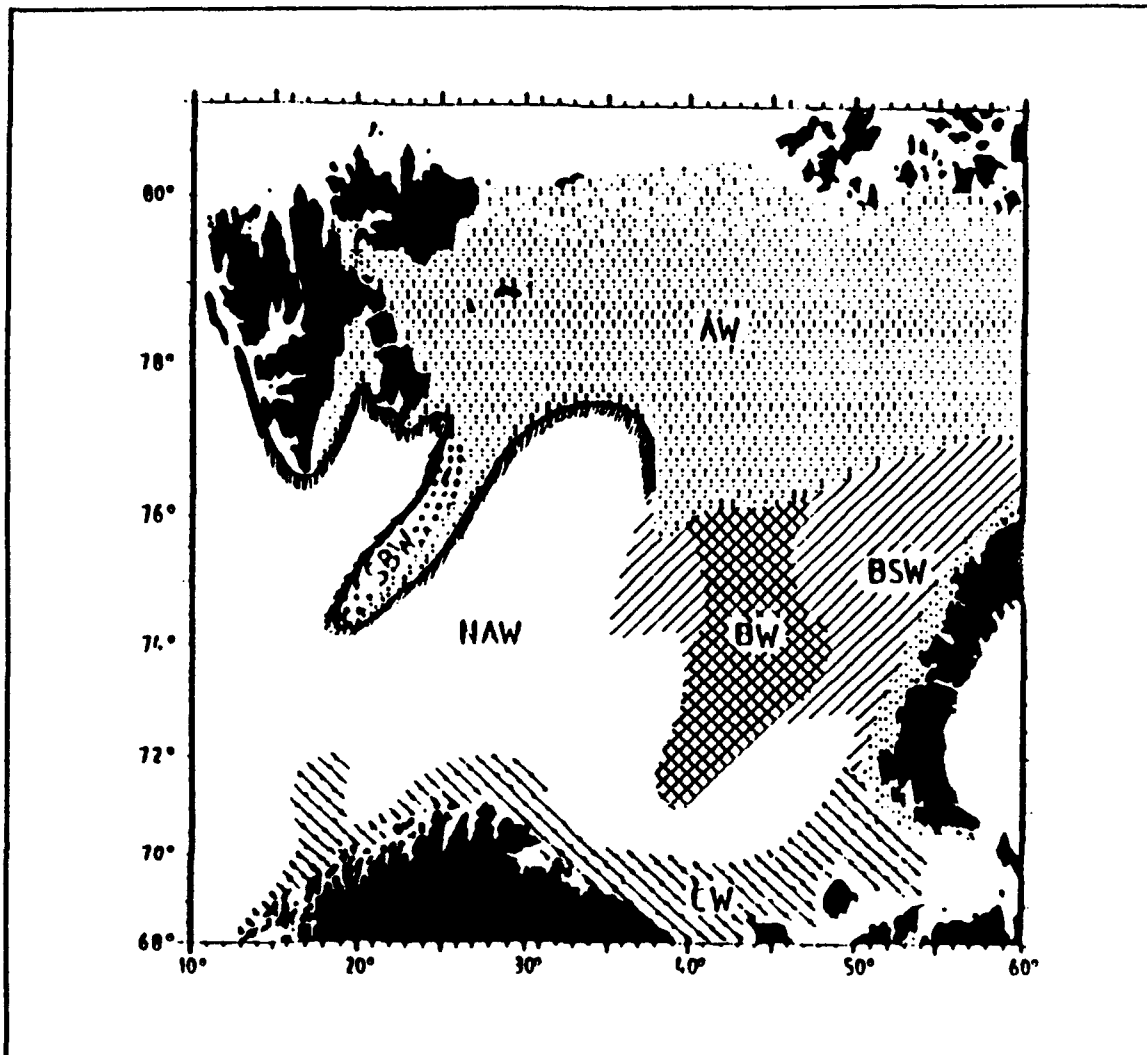


Figure 2.2: Barents Sea water masses [Ref. 6]. Water masses as described in the text.

The physical oceanography of the region plays a large role in controlling sound propagation [Ref. 7]. The region is shallow having an average depth of about 200 m. The bottom is rough in some areas and consists of a thin sediment overlying hard rock. The bathymetry and sound speed is highly range dependent. The shallow water causes many surface and bottom interactions in the acoustic propagation.

The sound speed profile varies spatially [Ref. 6]. The sound speed profile measured at the vertical line array is shown in Figure 2.3. This sound speed profile is a typical Barents Sea profile south of the front for the summer. The sound speed profile gradient is basically negative from surface to bottom with a shallow mixed layer region. The negative gradient tends to bend rays toward the bottom.

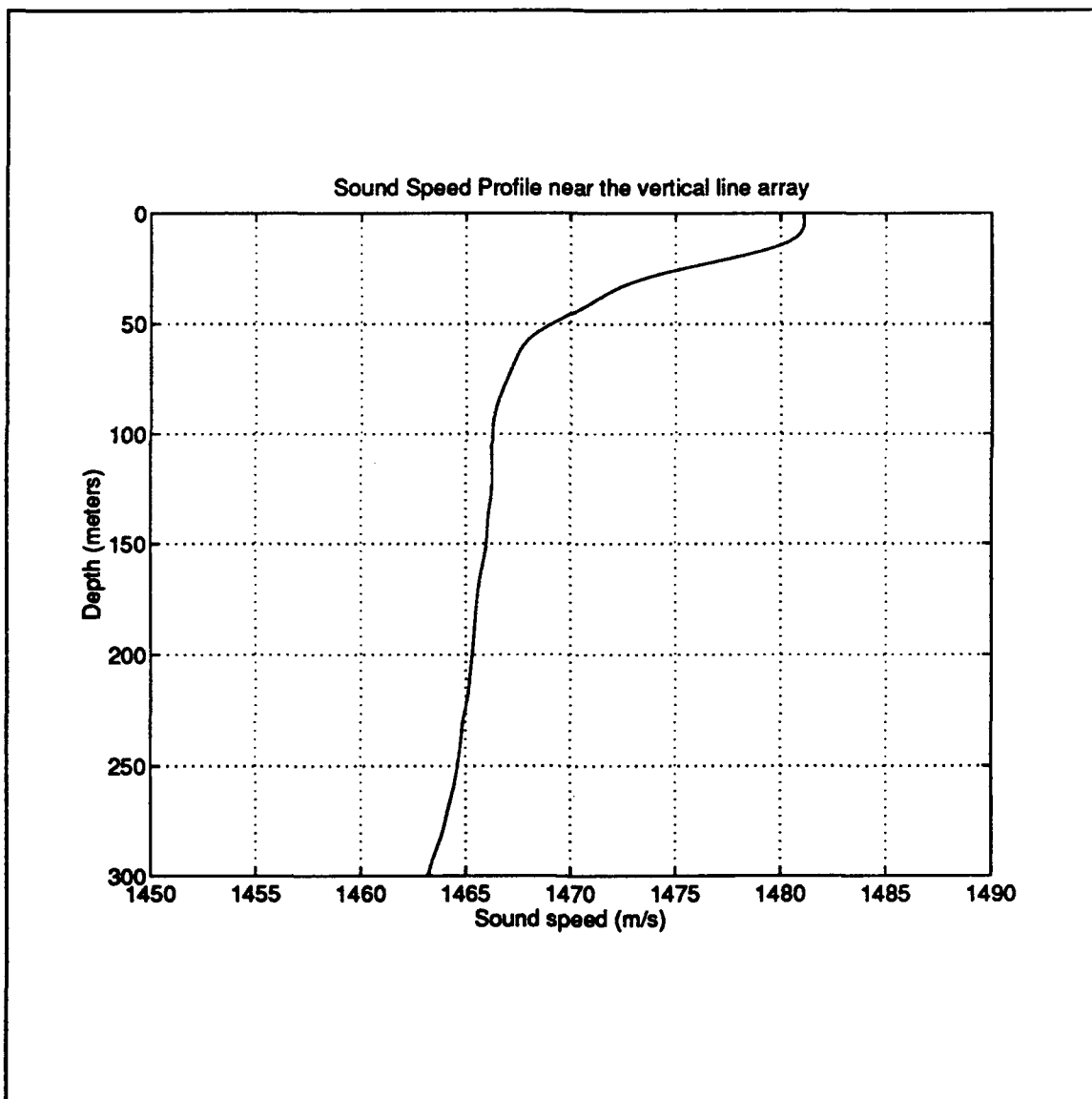


Figure 2.3: Sound speed profile near the vertical line array.

C. EQUIPMENT DESCRIPTION

The locations for moorings used in the experiment is shown in Figure 2.3 and the mooring locations given in Table II [Ref 9]. The moorings consisted of two 400 Hz transceivers (C and D), a 224 Hz source (A), and a vertical array of hydrophones (B). The characteristics of the sources is given in Table III. This thesis focus is on the signal processing of transmission from the 224 Hz source to the vertical array. The bathymetry between the 224 Hz source and vertical line array are shown in Figure 2.4.

Table II: Mooring Locations

Mooring	Latitude	Longitude	Depth (m)
(B) SE(a) VLA	74° 19.1512'N	23° 33.1438'E	275.0
(B) SE(b) VLA	74° 19.1996'N	23° 32.2960'E	275.0
(A) NE 224 Hz	74° 37.5535'N	23° 24.3755'E	142.0
(D) NW 400 Hz	74° 32.9152'N	21° 44.1043'E	176.0
(C) SW 400 Hz	74° 04.7337'N	22° 00.4605'E	380.0

Table III: BSPFEX Source Characteristics

Mooring	(A)	(C)	(D)
Frequency (Hz)	224	400	400
Source Level (dB) ref μPa	183	183	183
Bandwidth (Hz)	16	100	100
Duration (s)	118.25	132.86	132.86
Cycles/digit	14	4	4
Number of digits	63	511	511
Sequence length (s)	30	24(+2)	24(+2)
Repetition cycle	2.5,7.5,...	0,10,20,...	5,15,25,...

The 224 Hz source mooring is depicted in Figure 2.5 [Ref 10]. The source consisted of quarter wavelength resonant tubes driven by a piezoelectric transducer. A phase encoded signal (which is discussed in detail in Chapter III), was transmitted from the 224 Hz source and received on the vertical line array.

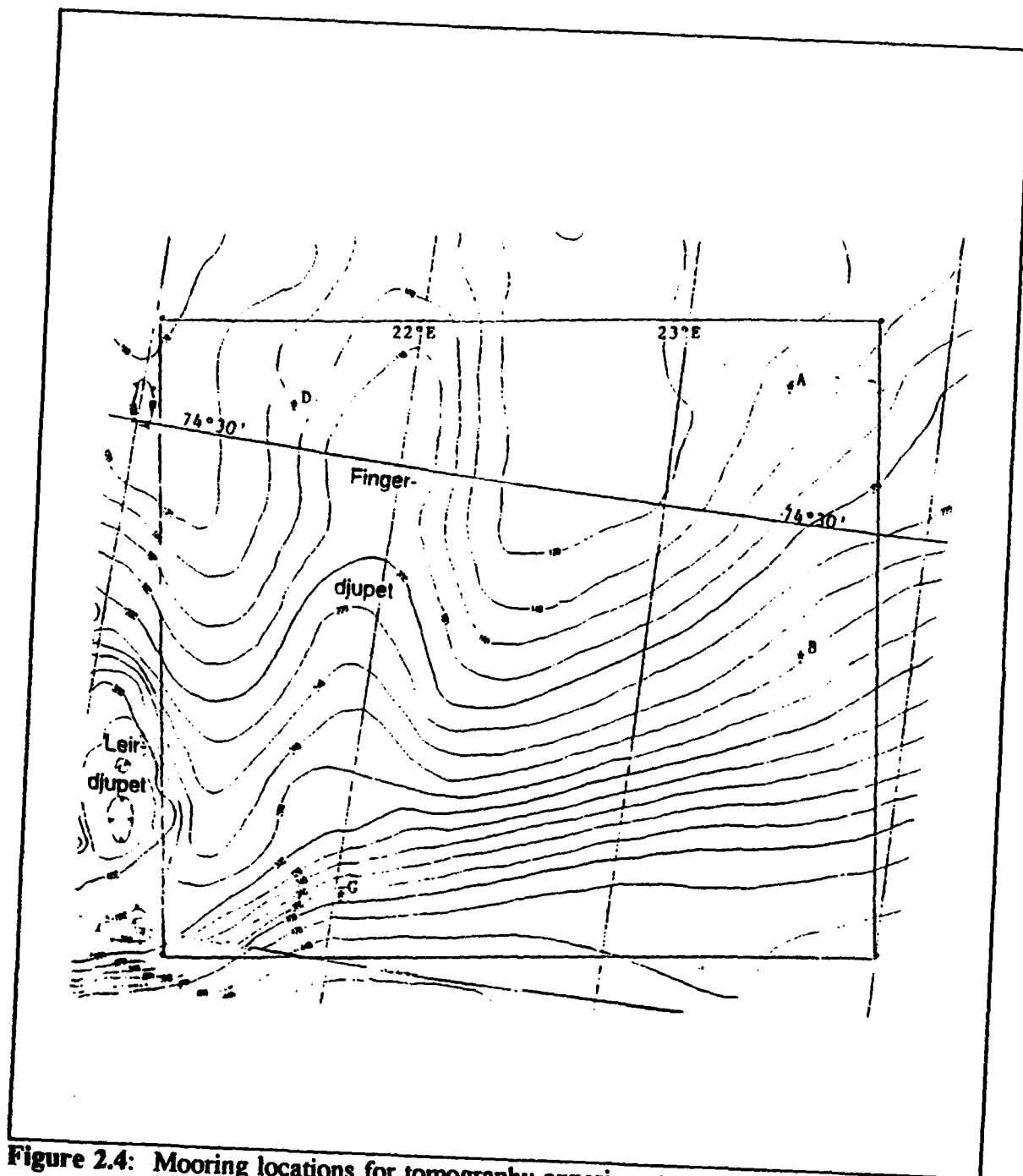


Figure 2.4: Mooring locations for tomography experiment.

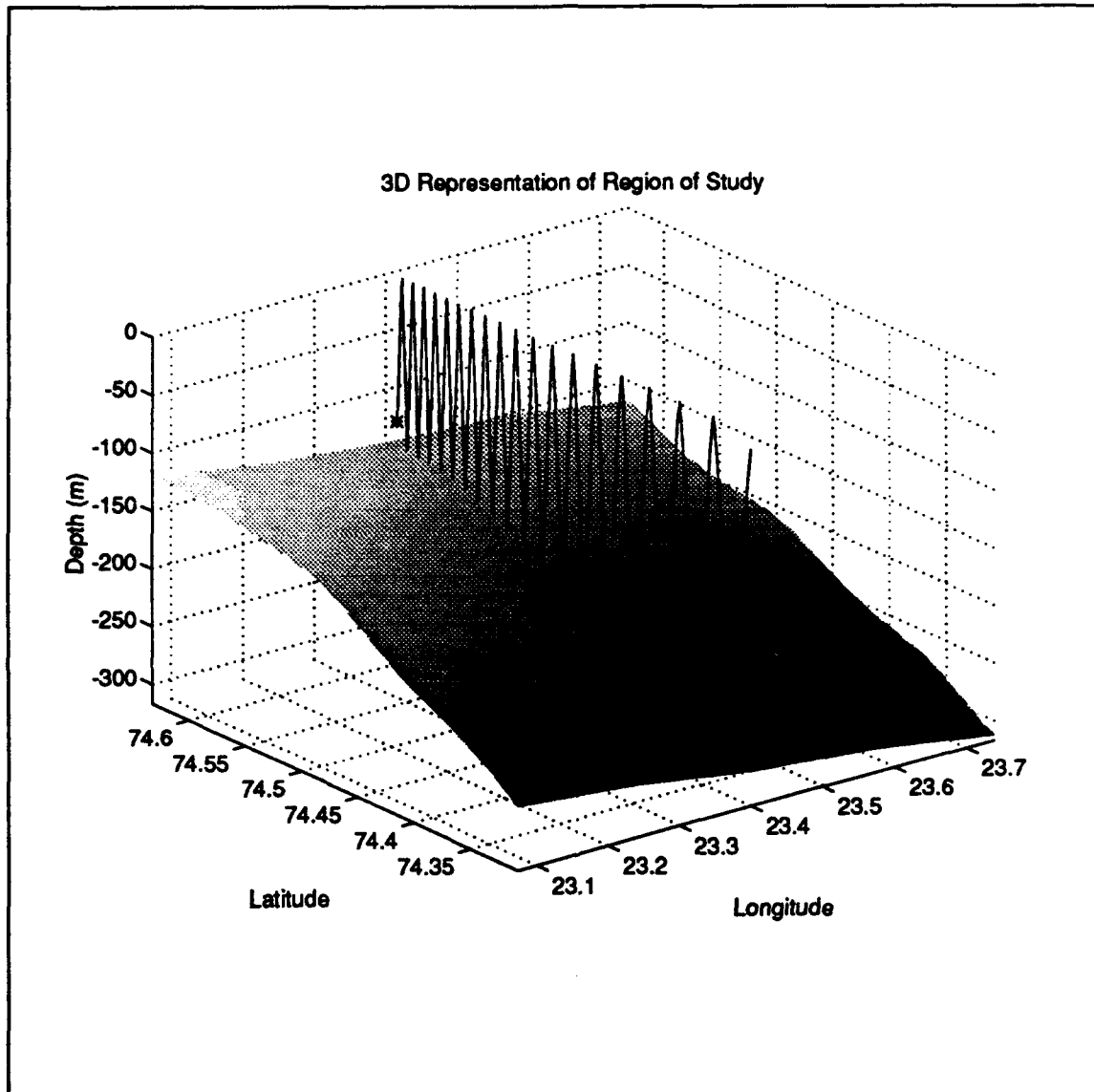


Figure 2.5: Three dimensional representation of transmission path for the tomography experiment.

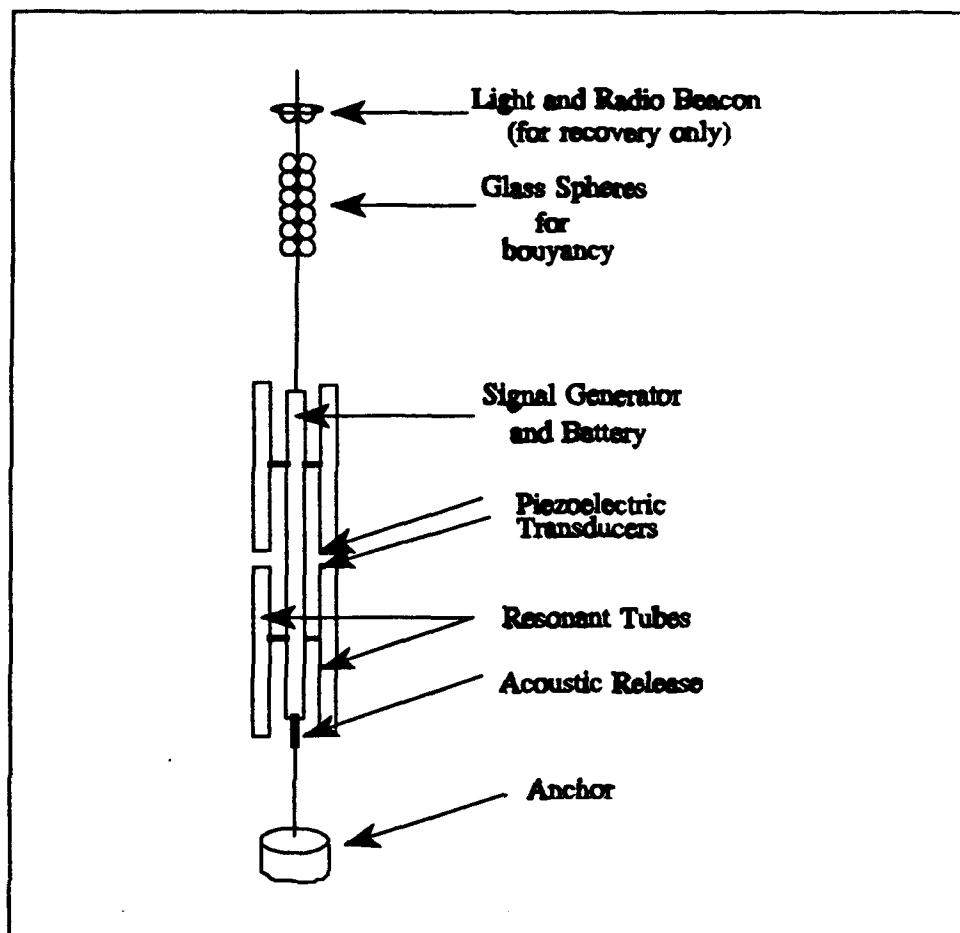


Figure 2.6: 224 Hz source mooring configuration.

The vertical line array is shown in Figure 2.7 [Ref. 11]. The array consisted of 16 hydrophones spaced 10 meters apart. The hydrophones have a sensitivity of -160 dB re V/ μ Pa. The mooring was designed to acoustically decouple the surface buoy from the array and minimize the effect of surface waves on mooring motion. The surface buoy contained an RF Ethernet system [Ref. 11] which transmitted the digitized data to the

ship. On the ship the data was stored on tape for later analysis. Some hydrophones experienced a loss in sensitivity due to an electrical problem. These hydrophones were later identified and were compensated for in the analysis of the data.

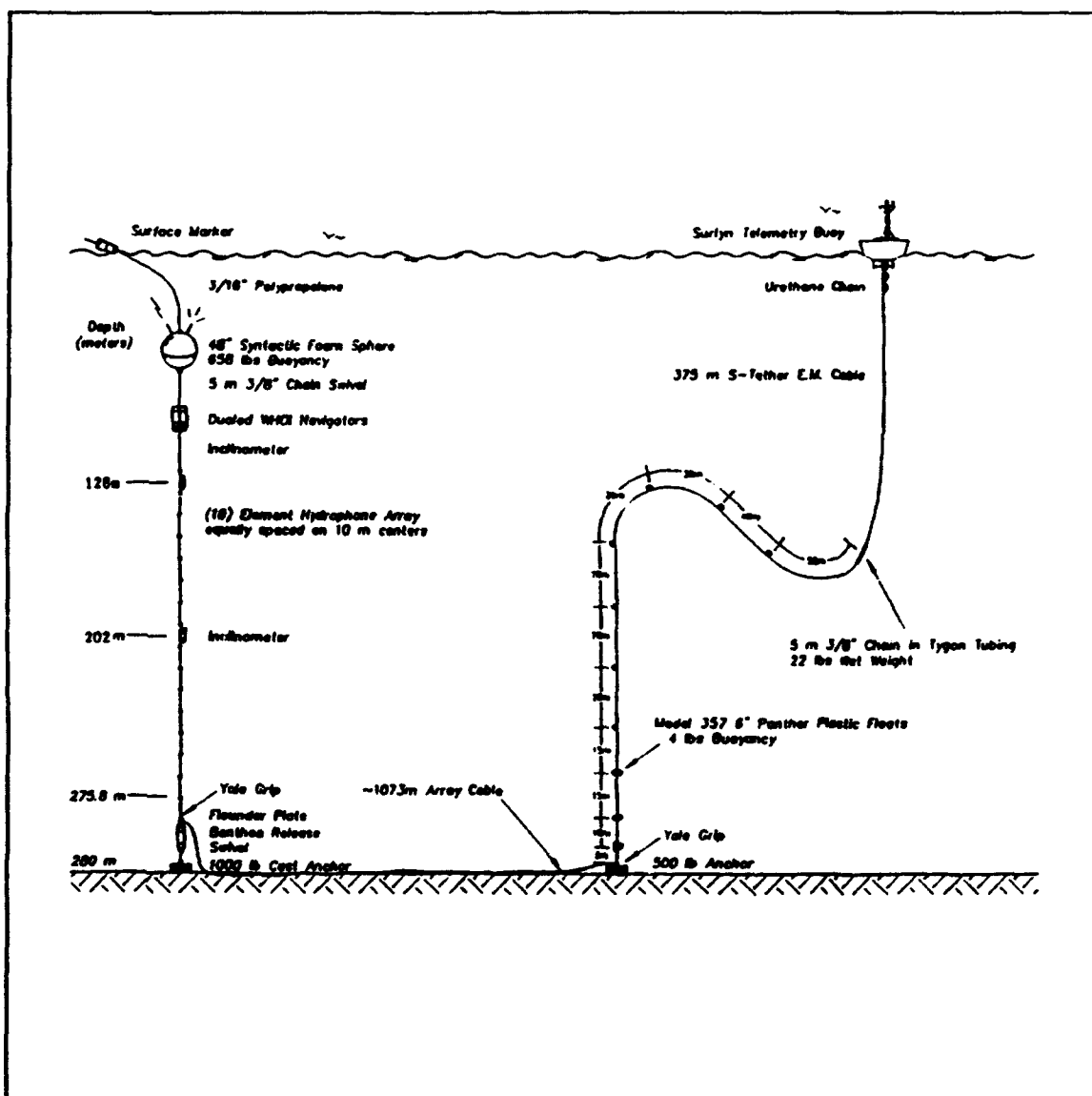


Figure 2.7: Diagram of the WHOI-NPS vertical line array used for the Barents Sea Polar Front Experiment [Ref. 11].

III. ACOUSTIC TOMOGRAPHY THEORY

A. TOMOGRAPHY PROBLEM OVERVIEW

The acoustic tomography problem consists of two parts, the forward problem and the inverse problem [Ref 2]. The forward problem establishes the physical relationship between data and the unknown structure. The inverse problem consists of estimating the unknown structure using data collected.

For acoustic tomography, the forward problem consists of a detailed analysis of the expected acoustic propagation for the area to be studied. This modeling of the environment determines the path of propagation and the expected arrival times for acoustic signals. Figure 3.1 shows a simplified view of the forward problem. Note that

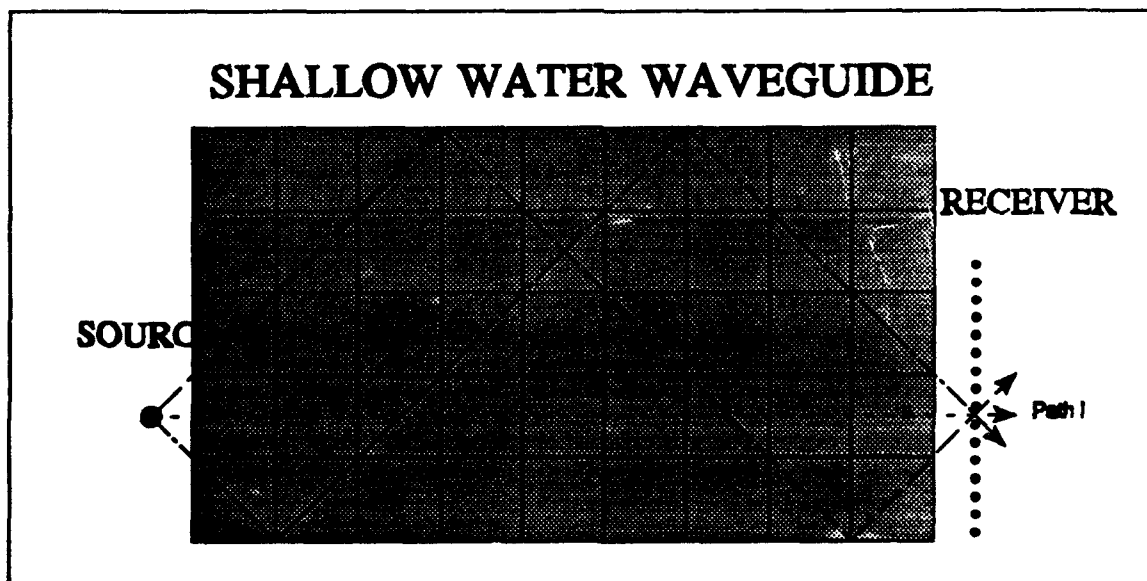


Figure 3.1: Simplified picture of shallow water tomography problem. There are many paths between source and receivers.

two of the paths have the same path length. Even with a background field that has a range dependent sound speed profile, two arrivals may occur too close together in time to distinguish. For the worst case, an isovelocity sound speed profile, there would be two arrivals at the same time. To distinguish these different arrivals, upward and downward propagating sound waves must be distinguished. Therefore in shallow water tomography, an array of hydrophones is often necessary for to separate the arrivals at different angles [Refs.3, 4].

The sound velocity field can be thought of as the sum of a background sound field with a sound speed perturbation [Ref 12],

$$c(x, y, z, t) = c_o(x, y, z) + \delta c(x, y, z, t) . \quad (3.1)$$

The travel time from the source to receiver along some path is given by,

$$\tau_i = \int_{path\ i} \frac{ds}{c(x, y, z, t)} . \quad (3.2)$$

If δc is small compared to c_o , then using a binomial expansion and substituting Equation 3.1 in to Equation 3.2 yields,

$$\tau_i \approx \int_{path\ i} \frac{ds}{c_o(x, y, z) \left(1 + \frac{\delta c(x, y, z, t)}{c_o(x, y, z)} \right)} . \quad (3.3)$$

Equation 3.3 can be approximated as

$$\tau_i \approx \int_{path\ i} \left(\frac{1}{c_o(x, y, z)} - \frac{\delta c}{c_o^2(x, y, z)} \right) ds. \quad (3.4)$$

The arrival time can now be broken down into an expected arrival time $\tau_{i,0}$ and a perturbation $\delta\tau_i$ as.

$$\tau_i = \tau_{i,0} + \delta\tau_i. \quad (3.5)$$

The arrival time perturbation is then given by

$$\delta\tau_i = - \int_{path\ i} \frac{\delta c(x, y, z, t)}{c_o^2(x, y, z)} ds. \quad (3.6)$$

The inverse problem is then to determine δc from the arrival time perturbation $\delta\tau$. The determination of the time perturbation is then dependent on the solution of the forward problem which is given by,

$$\tau_{i,0} \approx \int_{path\ i} \frac{1}{c_o(x, y, z)} ds. \quad (3.7)$$

The data for the inverse problem is $\delta\tau_i$ as indicated by Equation 3.6. The data is the difference between the measured arrival time of acoustic signals and the model predicted arrival times. The model arrival times are used in the detection and identification of actual arrivals. The model arrival times focus in where to look for the expected arrivals. Two types of models were used, a ray (plane wave-like) propagation model and modal propagation model.

B. FORWARD PROBLEM

1. Plane Wave Propagation

Ray theory is the result of an approximate solution to the linearized wave equation [Ref. 12]. The wave equation is given by

$$\nabla^2 p - \frac{\omega^2}{c^2} \frac{\partial^2 p}{\partial t^2} = -4\pi\delta(\vec{r} - \vec{r}_o) e^{j\omega t}, \quad (3.8)$$

where $\vec{r}_o = (x_o, y_o, z_o)$ is the source location and the sound speed and pressure can vary spatially and temporally. A solution to the wave equation is

$$p(x, y, z, t) = A(x, y, z) e^{j\omega(t - \Gamma(x, y, z)/c_1)}, \quad (3.9)$$

where A is the pressure amplitude, c_1 is a constant phase speed, and Γ has units of length.

The direction of travel for the wave is given by $\nabla\Gamma$. Substituting Equation 3.9 in to 3.8 yields:

$$\frac{\nabla^2 A}{A} - \left(\frac{\omega}{c}\right)^2 \nabla\Gamma \cdot \nabla\Gamma + \left(\frac{\omega}{c}\right)^2 - j\frac{\omega}{c_o} \left(2\frac{\nabla A}{A} \cdot \nabla\Gamma + \nabla^2\Gamma\right) = 0. \quad (3.10)$$

If the following approximations are made:

$$\left|\frac{\nabla^2 A}{A}\right| \ll \left(\frac{\omega}{c_o}\right)^2, \quad |\nabla^2\Gamma| \ll \frac{\omega}{c}, \quad \left|\frac{\nabla A}{A} \cdot \nabla\Gamma\right| \ll \frac{\omega}{c}, \quad (3.11)$$

then the wave equation can be approximated by:

$$\nabla\Gamma \cdot \nabla\Gamma = n^2 \quad , \quad n(x, y, z) = \frac{c_o}{c(x, y, z)} \quad , \quad (3.12)$$

where $n(x, y, z)$ is the index of refraction and c_o is an arbitrary reference sound speed. This is known as the Eikonal equation. The approximations physically mean:

1. The amplitude must change slowly compared to a wavelength.
2. The speed of sound must change slowly compared to a wavelength.

The behavior of $\nabla\Gamma$ can be found from

$$\frac{d}{ds} (\nabla\Gamma) = \nabla n. \quad (3.13)$$

The model used for ray tracing was the NOAA Hamiltonian Acoustic Raytracing Program for the Ocean (HARPO) [Ref. 14]. Work on the ray forward problem was done by LT John Mykyta, USN [Ref. 6]. Programs external to HARPO were used to perform eigenray searches and account for losses from spreading or boundary interactions. Spreading losses, surface scattering losses, and bottom losses were incorporated after the raytracing was completed [Ref 6].

2. Modal Propagation

Equation 3.8 can also be solved for normal modes. Expressing Equation 3.8 in cylindrical coordinates yields [Ref. 15]

$$\frac{1}{r} \frac{\partial}{\partial r} \left(r \frac{\partial}{\partial r} \right) P + \frac{\partial^2}{\partial z^2} P = -\frac{2}{r} \delta(r) \delta(z - z_o) e^{j\omega t}. \quad (3.14)$$

With separation of variables, the solution to Equation 3.14 can be expressed as

$$p(r, z) = \sum_{n=1}^{\infty} \frac{R_n(r) Z_n(z, r)}{\sqrt{r}}, \quad (3.15)$$

where Z_n represents normal modes and is a solution to a Helmholtz equation [Ref. 15]:

$$\frac{\partial}{\partial z} \left(\frac{1}{\rho_o(z)} \frac{\partial Z_n}{\partial z} \right) + \left(\frac{k^2(r, z)}{\rho_o(z)} - \frac{k_n^2(r)}{\rho_o(z)} \right) Z_n = 0, \quad (3.16)$$

where $k^2(r, z)$ is the wave number and $k_n^2(r)$ is the eigenvalue. Z_n also represents an orthonormal set which satisfies

$$\int \frac{Z_n Z_m}{\rho_o} dz = \delta_{nm}. \quad (3.17)$$

The radial component R_n satisfies [Ref. 15]:

$$\frac{d^2 R_m}{dr^2} + \left(k_m^2(r) + \frac{1}{4r^2} \right) R_m = - \sum_n [A_{mn}(r) R_n + 2B_{mn}(r)] \frac{dR_n}{dr}. \quad (3.18)$$

Neglecting $1/(4r^2)$ term and assuming adiabatic the solution becomes:

$$p(r, z) = e^{j\frac{\pi}{4}} \sqrt{2\pi} \sum_m \frac{Z_m(z_s, 0) Z_m(z, r)}{\sqrt{k_n r}} e^{j \int_0^r k_n(r') dr'}. \quad (3.19)$$

For normal mode modeling, mode coupling must be considered for significantly range dependent problems [Ref. 3].

C. SPACE-TIME SIGNAL PROCESSING

1. Temporal Signal Processing

In acoustic tomography, arrival times must be measured to within a few micro seconds. In order to achieve this accuracies, impulse-like signals are desirable with high signal-to-noise ratios [Refs. 4,12]. Impulses are ideal for mathematical modeling but are physically difficult to achieve with finite bandwidth sources whose peak power is limited. One solution is to use pulse compression techniques. The idea is to spread the energy out in the time domain efficiently using the available bandwidth of the source. At the receiver, the energy is combined or compressed to an impulse-like arrival. Coding schemes such as maximal-length sequences (m-sequences) have been used with success in a number of recent tomography experiments [Refs. 4,12].

M-sequences can be constructed from primitive polynomials [Ref. 16]. The signal for the 1992 Barents Sea tomography experiment [Ref. 4] was based on a sixth degree primitive polynomial given by

$$g(D) = D^6 + D + 1. \quad (3.20)$$

The output of the shift register (Figure 3.1) taken at any of the delays is a unique, periodic, binary sequence of length $N_m = 2^m - 1 = 63$ before repeating. The actual sequence used for the Barents Sea tomography experiment is shown in Figure 3.2.

M-sequences have a number of interesting properties which are outlined in a text book by Ziemer and Peterson [Ref 16]. An important property for the purposes of tomography is the autocorrelation of the sequence. If the binary sequence (0,1) is mapped to a (1,-1) sequence, then the normalized autocorrelation is shown in Figure 3.3. Note

that the autocorrelation consists of a triangle with a width of two digits and height of one and is everywhere else $1/N_m$.

Birdsall and Metzger (referred to as BM) [Ref. 17] have pioneered the use of m-sequences in acoustic tomography. To build a BM signal, the phase is encoded with the m-sequence. The phase-encoded signal is

$$s(t) = A \cos(2\pi f_o t + m(t) \theta_o) \quad (3.21)$$

where f_o is the carrier frequency, A is a constant amplitude, $m(t)$ is the m-sequence to be encoded, and θ_o is a constant. The constant θ_o can be chosen to maximize the relative power between the carrier and sidebands. The θ_o which maximizes the output signal-to-noise ratio is given by [Ref 17]

$$\theta_o = \tan^{-1}(\sqrt{N_m}) \quad (3.22)$$

which for the Barents Sea experiment was 82.8192 degrees [Ref. 4]. The frequency spectrum for the signal is shown in Figure 3.4. The complex envelope of the BM signal is [Ref. 4]

$$\tilde{s}(t) = A e^{jm(t)\theta_o} \quad (3.23)$$

The important feature of the autocorrelation of the complex envelope of the BM signal is the lack of sidelobes, making arrival time estimation of such a signal as accurate as possible. This is seen by computing the periodic autocorrelation as

$$R_{BB}(\tau) = \int_{T=N_m d} A e^{jm(t)\theta_0} A e^{-jm(t+\tau)\theta_0} d\tau, \quad (3.24)$$

where the integration is over one period ($T = N_m d$) of the m-sequence. BM show that this autocorrelation is 0 outside the main lobe as shown in Figure 3.5, i.e.

$$R_{BB}(\tau) = \begin{cases} A^2 T & \text{if } \tau = 0 \\ 0 & \text{if } |\tau| > d \end{cases} \quad (3.25)$$

Equation 3.24 can be converted to the frequency domain as

$$R_{BB}(f) = \tilde{S}(f) \tilde{S}^*(f) \quad (3.26)$$

where $S(f)$ is the fft of $s(t)$. Since beamforming was conducted in the frequency domain, temporal filtering was easily incorporated with Equation 3.26. Prior to processing, a replica of the signal $s(t)$ was converted through an fft to $S(f)$. The complex conjugate of $S(f)$ was then used for circular convolution in the frequency domain.

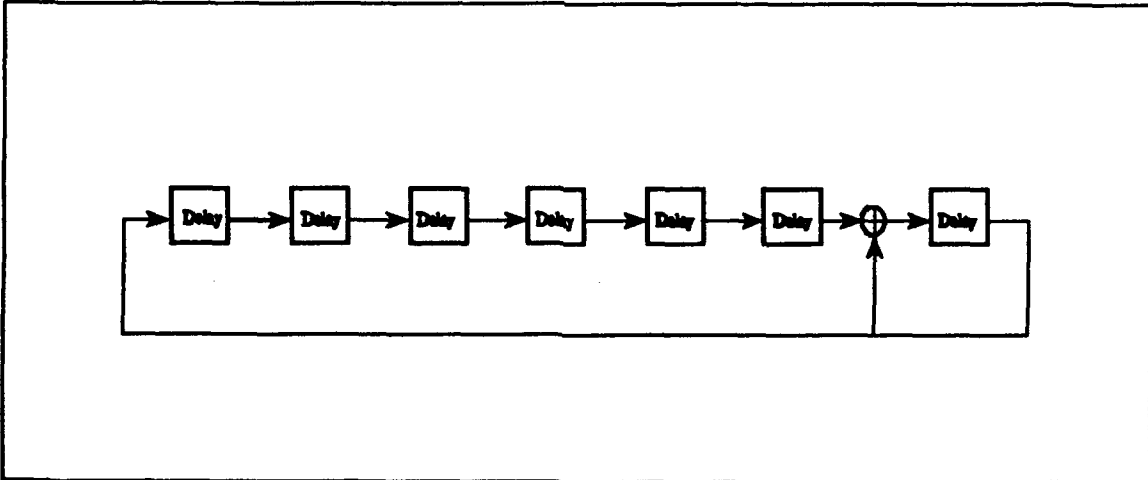


Figure 3.1: Delays for generating m-sequence (modulo 2 sum).

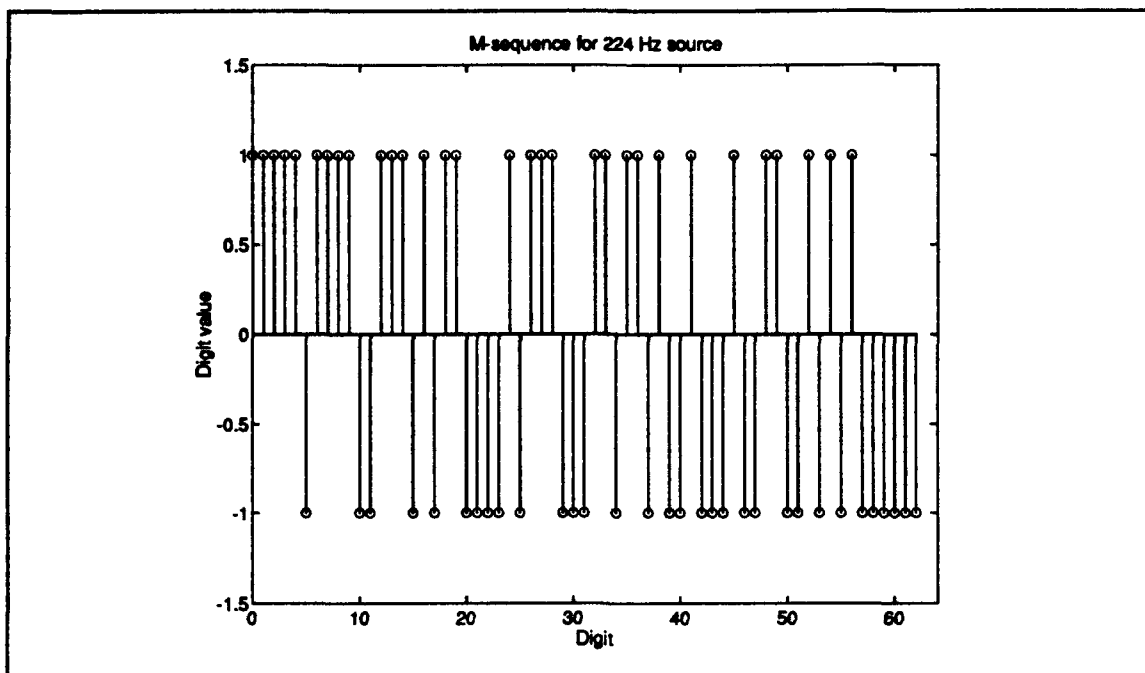


Figure 3.2: M-sequence code for 224 Hz source.

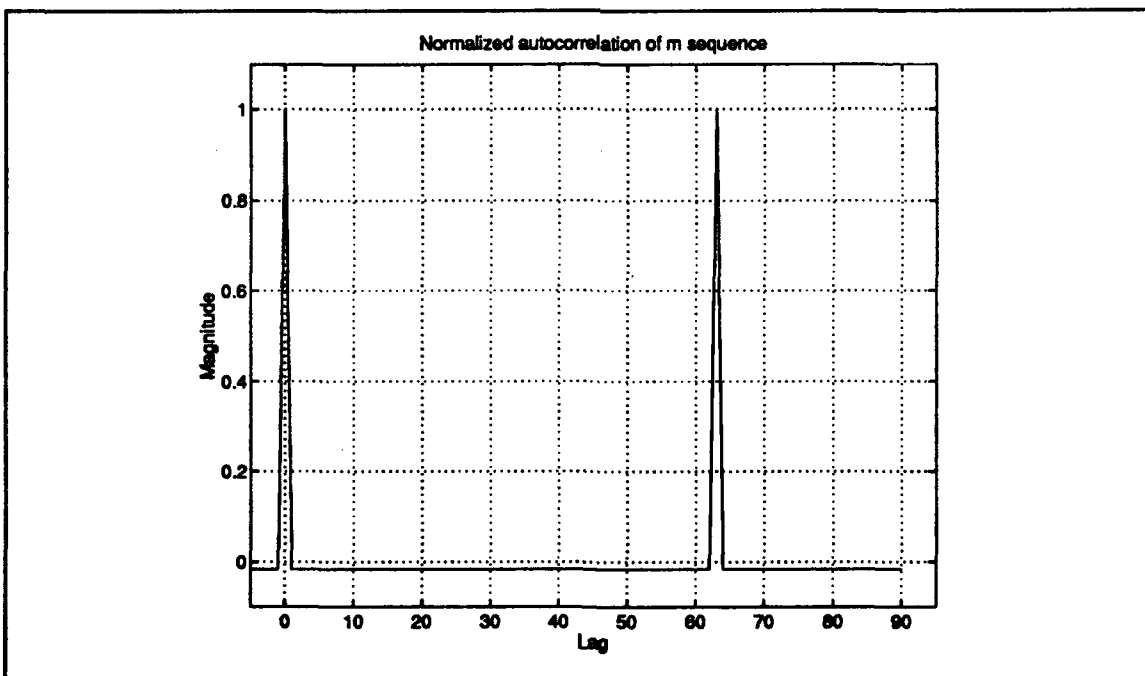


Figure 3.3: Autocorrelation property of m-sequence.

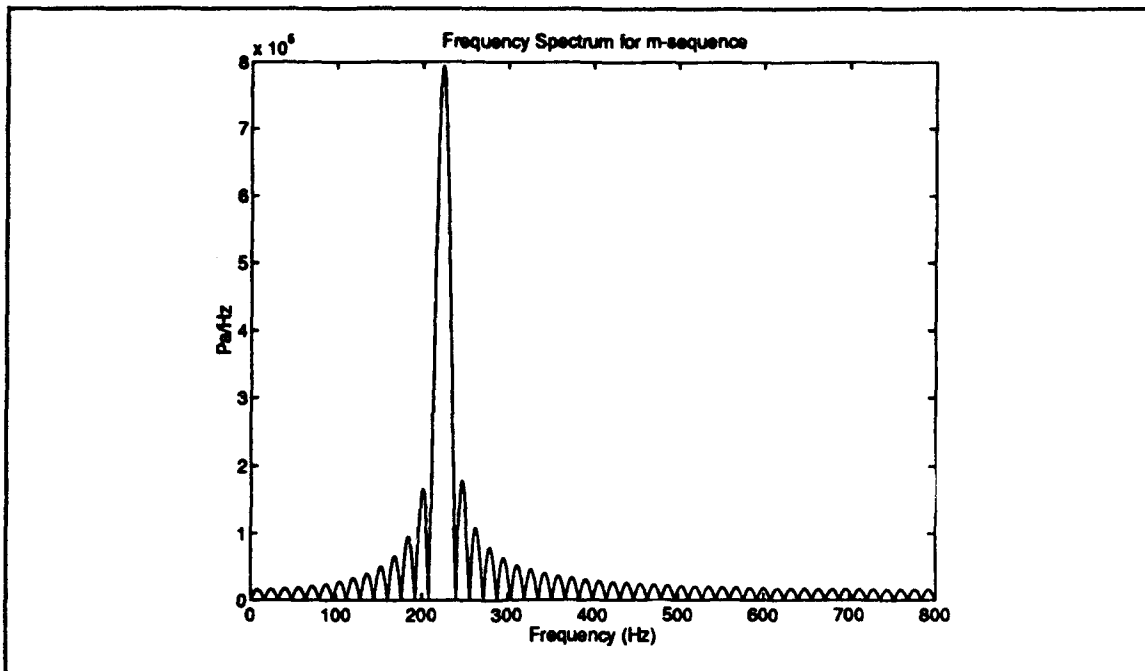


Figure 3.4: Coded signal frequency spectrum.

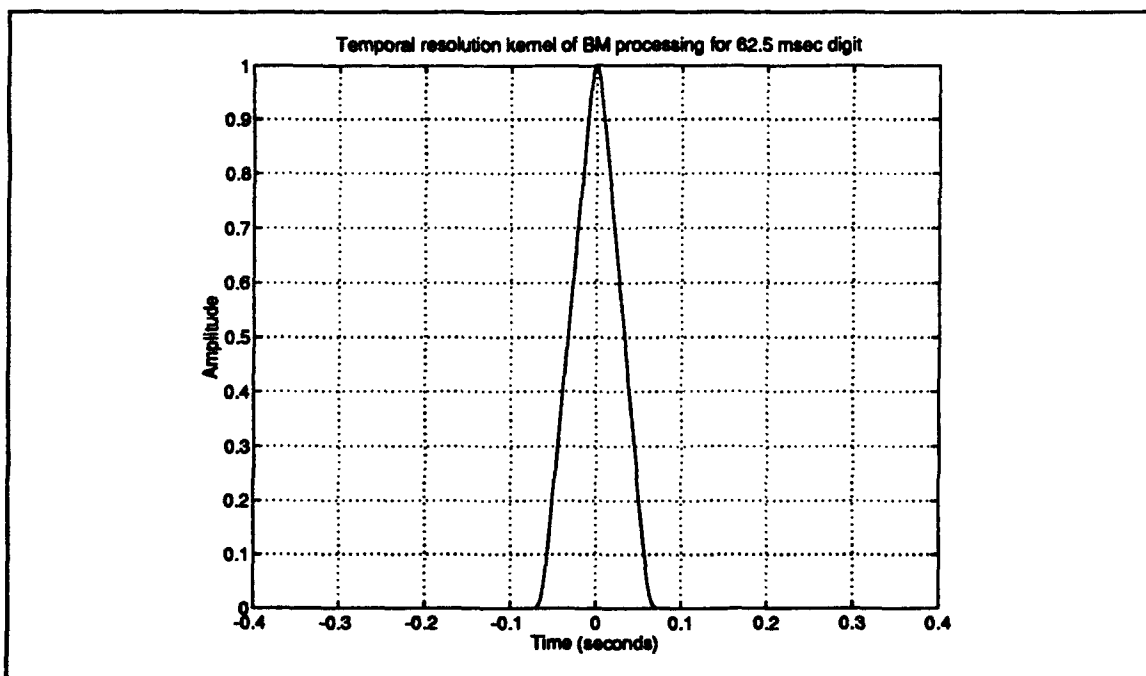


Figure 3.5: Temporal resolution kernel of BM processing for 62.5 msec digit [Ref. 4].

2. Spatial Signal Processing

a. Plane Wave Beamforming

The resolution and identification of individual rays can often be accomplished by plane-wave beamforming the outputs of individual hydrophones on a vertical array [Ref. 4]. The outputs of the hydrophones can be phase shifted to maximize the sensitivity in a particular direction. The complex envelope of the n^{th} ray, which is assumed to be a local plane wave acoustic signal with m-sequence phase modulation, is given by [Ref. 4]

$$\tilde{p}_n(t, \vec{x}) = a_n^r(\vec{x}) e^{\left[-j2\pi f \left(\frac{\vec{u} \cdot \vec{x}}{c} - t_n^r\right) + jm \left(t - \frac{\vec{u} \cdot \vec{x}}{c} - t_n^r\right)\right]}, \quad (3.27)$$

where $\vec{u} = (u, v, w)$ are the direction cosines with respect to the (x, y, z) axes and are given by

$$\begin{aligned} u &= \sin\theta \cos\psi \\ v &= \sin\theta \sin\psi \\ w &= \cos\theta \end{aligned} \quad (3.28)$$

in terms of the spherical angles θ and ψ . The Fourier transform of the complex envelope of the n^{th} ray's pressure field is

$$\tilde{p}_n(f, \vec{x}) = a_n^r(\vec{x}) S_m(f) e^{\left[-j2\pi f \left(\frac{\vec{u} \cdot \vec{x}}{c} + t_n^r\right)\right]} \quad (3.29)$$

where $S_m(f)$ is the Fourier transform of the complex envelope of the m-sequence phase encoded signal given by

$$S_m(f) = F\{e^{jm(t)\theta_0}\}. \quad (3.30)$$

The vertical array beamforming and associated m-sequence processing can be thought of as a spatial-temporal matched filter which as a transfer function is given by

$$B_{ray}(f, \vec{x}) = \sum_{h=1}^H \delta(z-z_h) \delta(x-x_r) \delta(y-y_r) S_m^*(f) e^{-j2\pi f \tau_h}, \quad (3.31)$$

where H is the number of hydrophone, z_h are the hydrophone depths, x_r and y_r are the coordinates of the vertical array, and τ_h is an adjustable time delay applied to each hydrophone. The complex envelope of the output of any general beamformer is given by

$$\tilde{Y}(f) = \int_{V_0} \tilde{P}(f, \vec{x}) \cdot B_{ray}(f, \vec{x}) dV_0 \quad (3.32)$$

where V_0 is the volume of the aperture or array. For the Barents Sea Tomography Experiment we have

$$\tilde{Y}(f) = a_n^r \sum_{h=1}^{16} e^{-j2\pi f \tau_h} S_m(f) S_m^*(f) e^{-j2\pi f \cos \theta_i z_h / c} e^{-j2\pi f t_n^r} \quad (3.33)$$

where a local coordinate system is assumed for the vertical array. If the time delays are adjusted for

$$\tau_h = -\frac{z_h}{c} \cos \theta_i, \quad (3.34)$$

we have a spatial-temporal matched plane-wave filter for the n^{th} ray. If the acoustic field is well modeled, different delays may be included such as wavefront curvature.

The uncertainty in the estimate for travel time depends on the signal to noise ratio [Ref. 4]. The standard deviation of the travel time estimation error is well modeled by

$$\sigma_t = \frac{d}{\sqrt{SNR}}, \quad (3.35)$$

where SNR is the signal-to-noise ratio and d is the digit width of the maximal length sequence modulating the phase of the transmitted signal. Equation 3.35 is valid for SNR greater than 10.

b. Mode Beamforming

The resolution and identification of individual normal modes can be accomplished by beamforming the outputs of individual hydrophones on a vertical array [Ref. 3,4]. Instead of time delaying the outputs by an appropriate amount (or phase shifting in the frequency domain) to plane-wave beamform for a ray, the amplitude of the mode at each of the hydrophones across the band of frequencies the signal occupies is matched. The temporal Fourier transform of the complex envelope of the n^{th} mode's pressure field is

$$\tilde{P}_n(f, \vec{x}) = a_n(x, y) Z_n(f, x, y, z) S_m(f) e^{-j2\pi f t_n^m(x, y)} \quad (3.36)$$

where $Z_n(f, x, y, z)$ is the n th local mode function which satisfies orthogonality in depth at all (x, y) and $S_m(f)$ is the Fourier transform of the complex envelope of the m -sequence phase-encoded signal as in the ray case. The vertical array and m -sequence processing

can be thought of as the spatial-temporal matched filter and has a transfer function given by

$$B_{mode}(f, \vec{x}) = \sum_{h=1}^H \delta(z - z_h) \delta(x) \delta(y) Z_n(f, x, y, z) S_m^*(f) \quad (3.37)$$

where H is the number of hydrophones and z_h are the hydrophone depths. The complex envelope of the output of the mode beamformer is

$$\tilde{Y}(f) = \int_{V_o} \tilde{P}(f, \vec{x}) \cdot B_{mode}(f, \vec{x}) dV_o. \quad (3.38)$$

For the Barents Sea Tomography Experiment the modal beamformer can be written as

$$\tilde{Y}(f) = \sum_{h=1}^{16} a_n Z_n(f, z_h) Z_n(z) S_m(f) S_m^*(f) e^{-j2\pi f t_n^m}. \quad (3.39)$$

The assumption that the modes are orthogonal over the array aperture leads to errors since the array only covers a portion of the water column. Shang [Ref. 15] suggests a least squares approach to modal beamforming. The least square problem is to find weights $A(f)$ such that the estimated field matches the measured field. The derivation for these weights $A(f)$ are shown here for completeness [Ref 18]. Assuming that the estimator $A(f)$ is linearly related to the observations yields

$$\hat{A} = Bd, \quad (3.40)$$

where d is the data, and B is a matrix to be determined. The error is given by:

$$e = \hat{A} - A. \quad (3.41)$$

The covariance of the error is

$$C_e = E[ee^T]. \quad (3.42)$$

The constant B is to be chosen to minimize C_e . The covariance of the error can be written as

$$\begin{aligned} C_e &= E[(Bd-A)(Bd-A)^T] \\ &= E[(Bd-A)(d^T B^T - A^T)] \\ &= E[Bdd^T B^T - Ad^T B^T - BdA^T + AA^T] \\ &= BC_d B^T - C_{Ad} B^T - BC_{Ad}^T + C_A, \end{aligned} \quad (3.43)$$

or equivalently as

$$C_e = (B - C_{Ad} C_d^{-1}) C_d (B - C_{Ad} C_d^{-1})^T - C_{Ad} C_d^{-1} C_{Ad}^T + C_A. \quad (3.44)$$

The minimization of C_e gives ,

$$B = C_{Ad} C_d^{-1}. \quad (3.45)$$

Substituting Equation 3.45 in to Equation 3.40 yields

$$\hat{A} = C_{Ad} C_d^{-1} d \quad (3.46)$$

where C_{Ad} the covariance A and d , and C_d is the covariance of the data d .

Assuming that the data can be represented as

$$d = M(z, f) A(f) + v_n(z, f) \quad (3.47)$$

where $M(z, f)$ is a matrix of mode weights at a hydrophones, $A(f)$ is a matrix of amplitudes, and $v_n(z, f)$ is noise associated with the observation at a hydrophone. The modes weights matrix is written as

$$M(z, f) = \begin{bmatrix} M_{1,0} & M_{2,0} & M_{3,0} & \cdot & \cdot & \cdot & M_{m,0} \\ M_{1,1} & M_{2,1} & M_{3,1} & \cdot & \cdot & \cdot & M_{m,1} \\ \cdot & \cdot & \cdot & \cdot & \cdot & \cdot & \cdot \\ \cdot & \cdot & \cdot & \cdot & \cdot & \cdot & \cdot \\ M_{1,15} & M_{2,15} & M_{3,15} & \cdot & \cdot & \cdot & M_{m,15} \end{bmatrix} \quad (3.48)$$

where the first subscript indicates mode number and the second indicates hydrophone number. The amplitude matrix is written as

$$A(f) = \begin{bmatrix} A_1 \\ A_2 \\ \cdot \\ \cdot \\ \cdot \\ A_m \end{bmatrix} \quad (3.49)$$

where the subscript indicates mode number. The least-squares problem is then to find the amplitude $A(f)$ where

$$\hat{A} = A(d) . \quad (3.50)$$

The solution to 3.50 is given by equation 3.42. The remaining portion of the problem is to find C_{Ad} and C_d . C_{Ad} can be found as follows:

$$\begin{aligned} C_{Ad} &= E[A(MA+v)^T] \\ &= E[A(A^T M^T + v^T)] \\ &= E[AA^T M^T + Av^T] \\ &= C_A M^T + C_{Av}. \end{aligned} \quad (3.51)$$

C_d is found as follows:

$$\begin{aligned} C_d &= E[(MA + v)(MA + v)^T] \\ &= E[(MA + v)(A^T M^T + v^T)] \\ &= E[MAA^T M^T + vA^T M^T + MAV^T + vv^T] \\ &= MC_A M^T + C_{Av} M^T + MC_{Av} + C_v. \end{aligned} \quad (3.52)$$

If the noise v and modal amplitudes are assumed to be uncorrelated, then Equation 3.52 simplifies to

$$C_d = MC_A M^T + C_v. \quad (3.53)$$

The solution can now be written by substituting Equations 3.53 and 3.51 into Equation 3.42 which yields

$$\hat{A} = (C_A M + C_{Av})(MC_A M^T + C_v)^{-1} d. \quad (3.54)$$

Equation 3.54 can be manipulated into a more familiar form of

$$\hat{A} = (C_A^{-1} + M^T C_v^{-1} M)^{-1} M^T C_v^{-1} d, \quad (3.55)$$

where C_A represents any a priori information, C_v is the covariance of the noise, and C_d represents the covariance of the error in the estimate.

The acoustic field at the array is described in a least-squares sense as

$$\hat{d} = \sum_m M(z, f) \hat{A}(f), \quad (3.56)$$

where $\hat{A}(f)$ was estimated as shown in Equation 3.55. The best beamformer in a least-squares sense is then described by

$$\tilde{Y}(f) = \sum_{n=1}^{16} a_n Z_n(f, z_h) Z_n(z) S_m(f) S_m^*(f) \hat{A}(f) e^{-j2\pi f t_n^*}. \quad (3.57)$$

As with Equation 3.39, the beamformer is summed over the 16 hydrophones.

IV. PERFORMANCE PREDICTIONS

A. PLANE WAVE PREDICTIONS

The hydrophone array used for the Barents Sea tomography experiment consisted of 16 elements separated by 10 meters as shown in Figure 2.7. The beam pattern for the array at 224 Hz is shown in Figure 4.1. Note the grating lobes are at plus and minus 40 degrees. These are caused by the spatial undersampling by the array. The 224 Hz frequency has a wavelength of approximately 6.5 meters and would require a hydrophone spacing less than 3.25 meters to prevent grating lobes. The grating lobes are acceptable because the arrivals are separated in both time and space. Thus energy coming in through a grating lobe will not interfere temporally with the beamformed arrival. A rectangular window was chosen for the array to achieve the narrowest beamwidth possible for arrival identification. The -3 dB beamwidth for the array is 2 degrees at 224 Hz.

Chapter II showed the physical setup for the tomography experiment. The sound speed profile (Figure 2.3) is basically a negative gradient. The effect of this environment for plane waves was modeled by John Mykyta using HARPO and other codes [Ref 6,14]. A plane wave assumption leads to errors since in a non-isovelocity environment the arrivals will not be plane waves. To show the effect of plane wave beamforming when the incoming wave is not a plane wave, a one millisecond delay was allowed over the array. The result is shown in Figure 4.2. The effect is that sensitivity is reduced by one dB and the sidelobes are higher. If the environment is known well enough, these

wavefront curvatures can be taken in to account as pointed out in Equation 3.19. Several approaches are available. The corrections for wavefront curvature can be done using only the background environmental model or after each inversion, produce a new environmental model for wavefront correction.

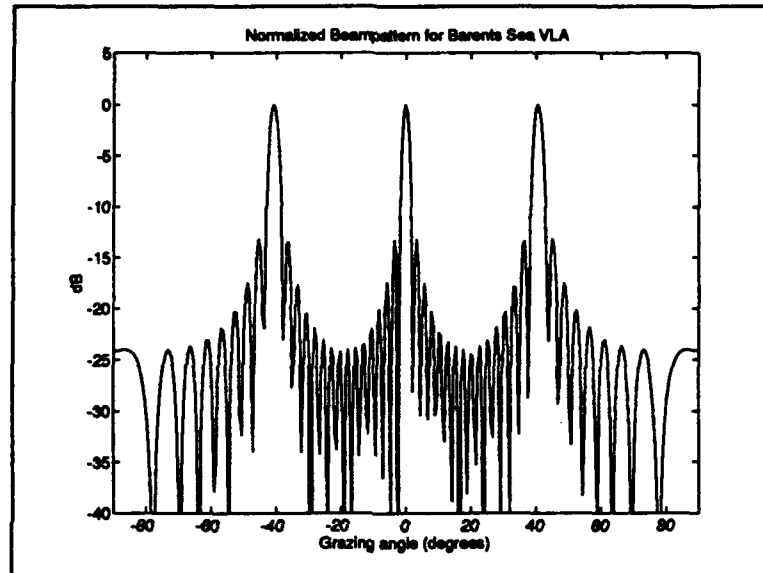


Figure 4.1: Plane wave beam pattern for Barents Sea VLA at 224 Hz.

The actual amount of wavefront curvature varies with arrival angle. An example of the predicted wavefront curvature is shown in Figure 4.3. The wavefront curvature predictions were done by John Mykyta using HARPO [Ref. 6]. These predictions were made while determining the arrival structure at the array.

The difference between the predicted arrivals and the actual arrivals is used to find the sound speed perturbations. The predicted arrival structure is shown in Figure 4.4.

While the arrival structure appears to be smooth, it does not take in to account the beam pattern of the array. A more representative picture of the arrival structure is shown in Figure 4.5. Here the arrivals within a one degree bin are shown. For low angles, there is little separation between the arrivals, but for the higher angles (greater than plus or minus eight degrees), there is sufficient temporal separation to resolve more than one arrival. Figure 4.6 shows the predicted beamformed arrivals. Thus for higher angles multiple arrivals should be seen. Arrivals are indicated by the higher (red) amplitude regions. This figure was produced by beamforming synthetic data. Multiple arrivals are evident in higher angles.

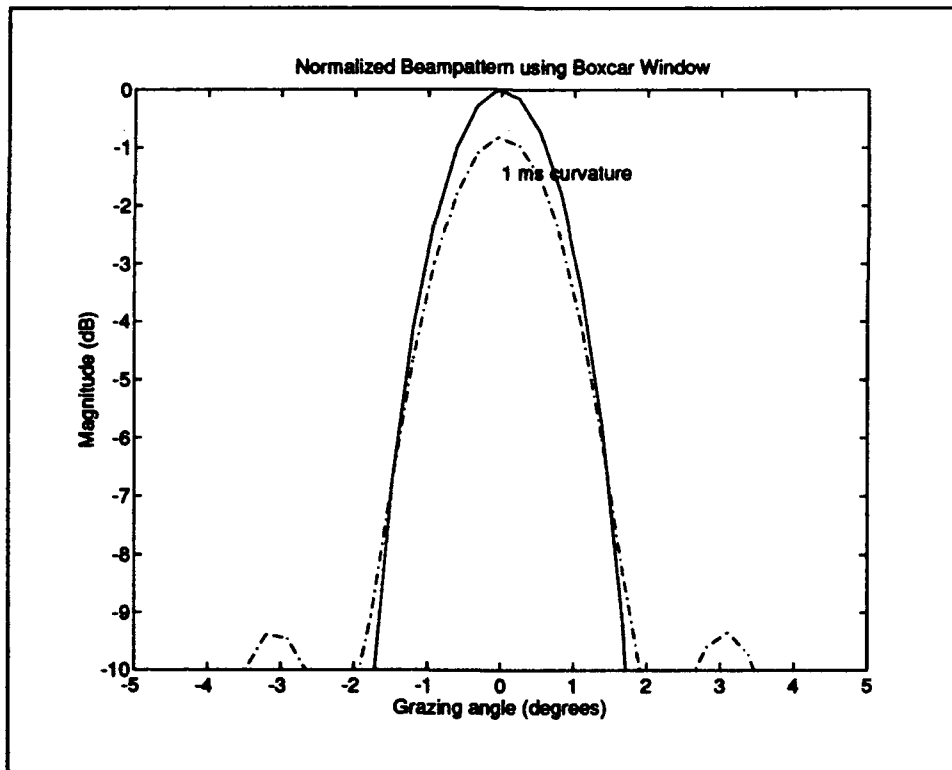


Figure 4.2: Wavefront curvature degradation prediction.

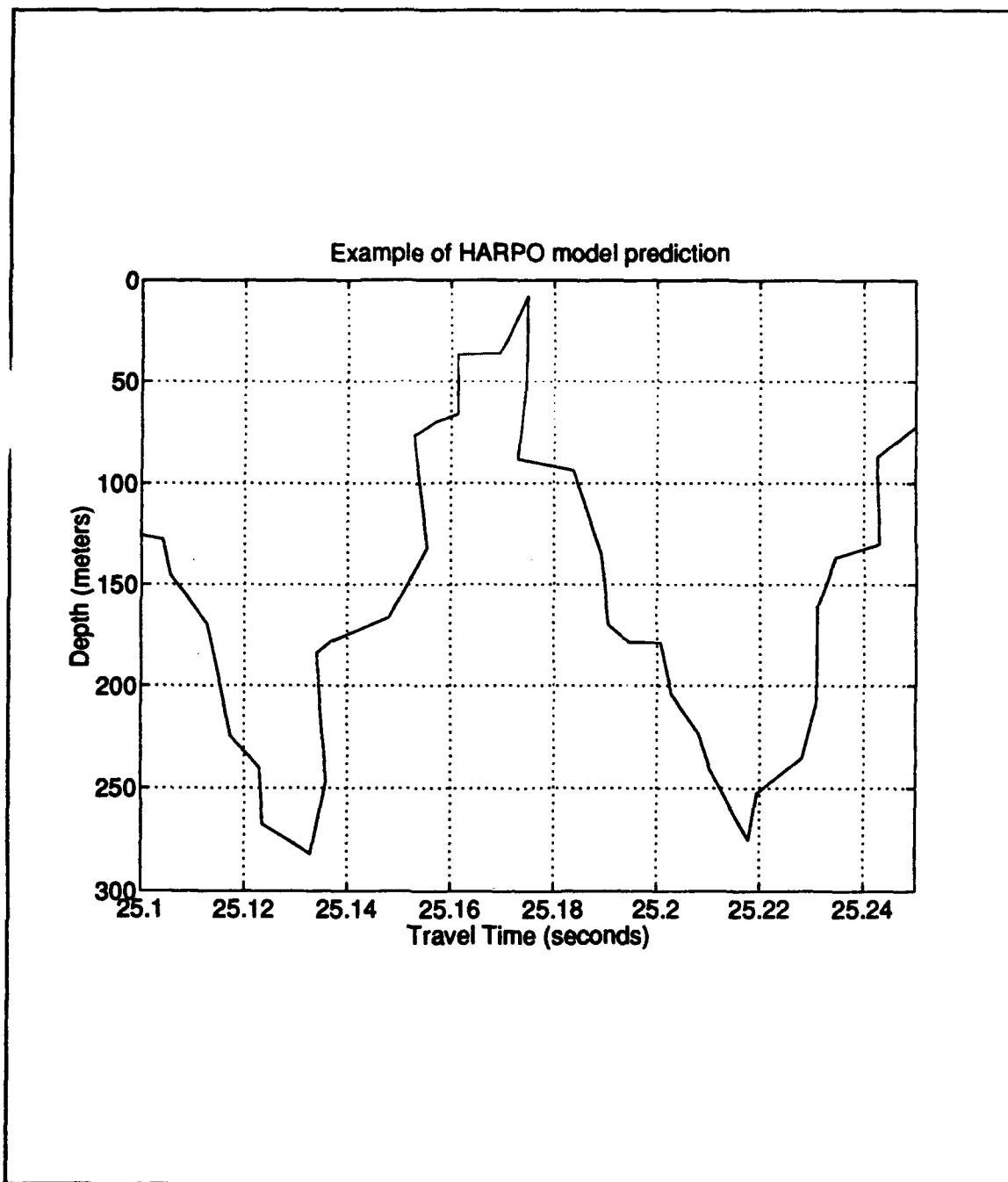


Figure 4.3: Example of predicted wavefront curvature.

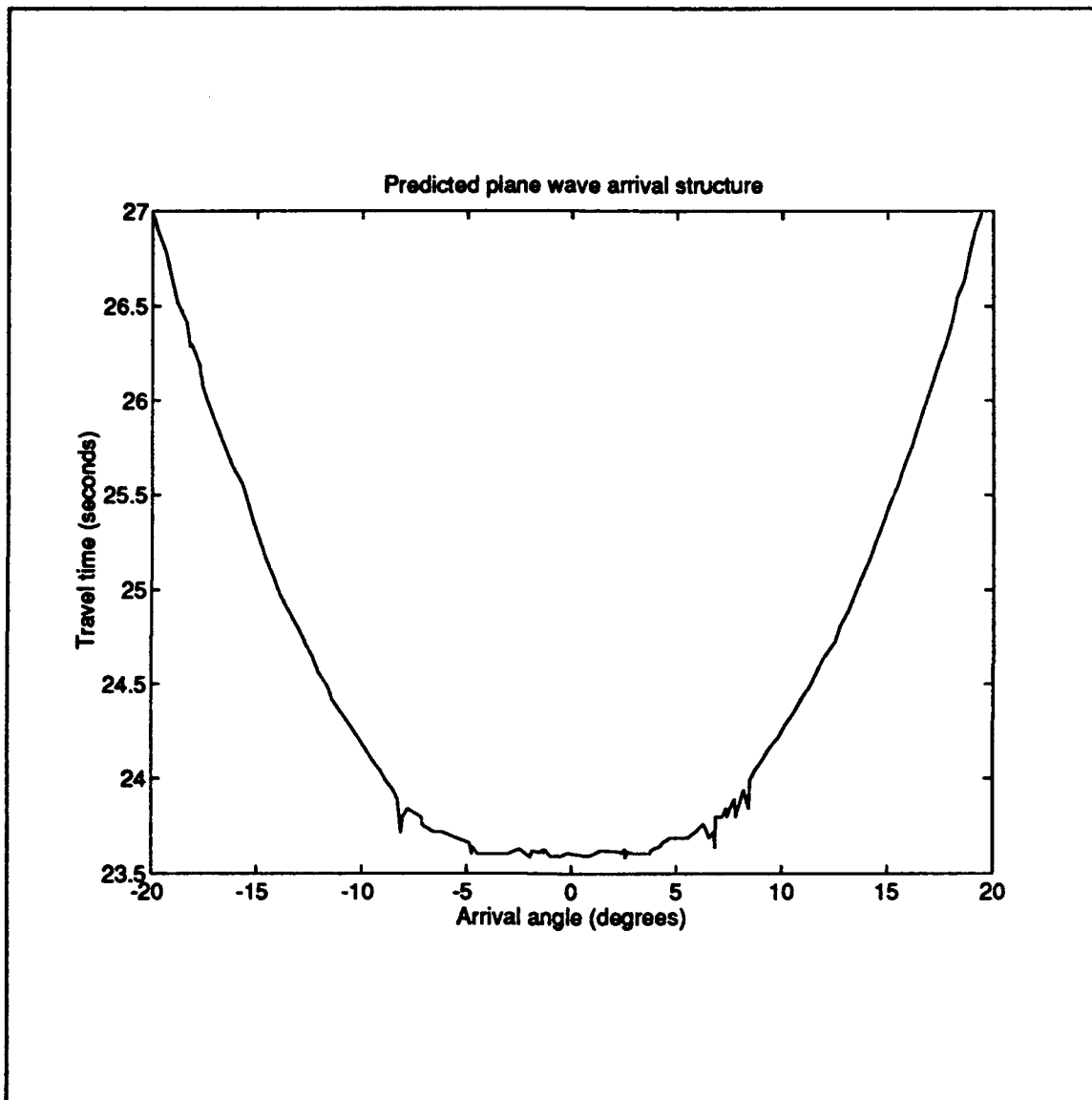


Figure 4.4: Predicted plane wave arrival structure [Ref. 6].

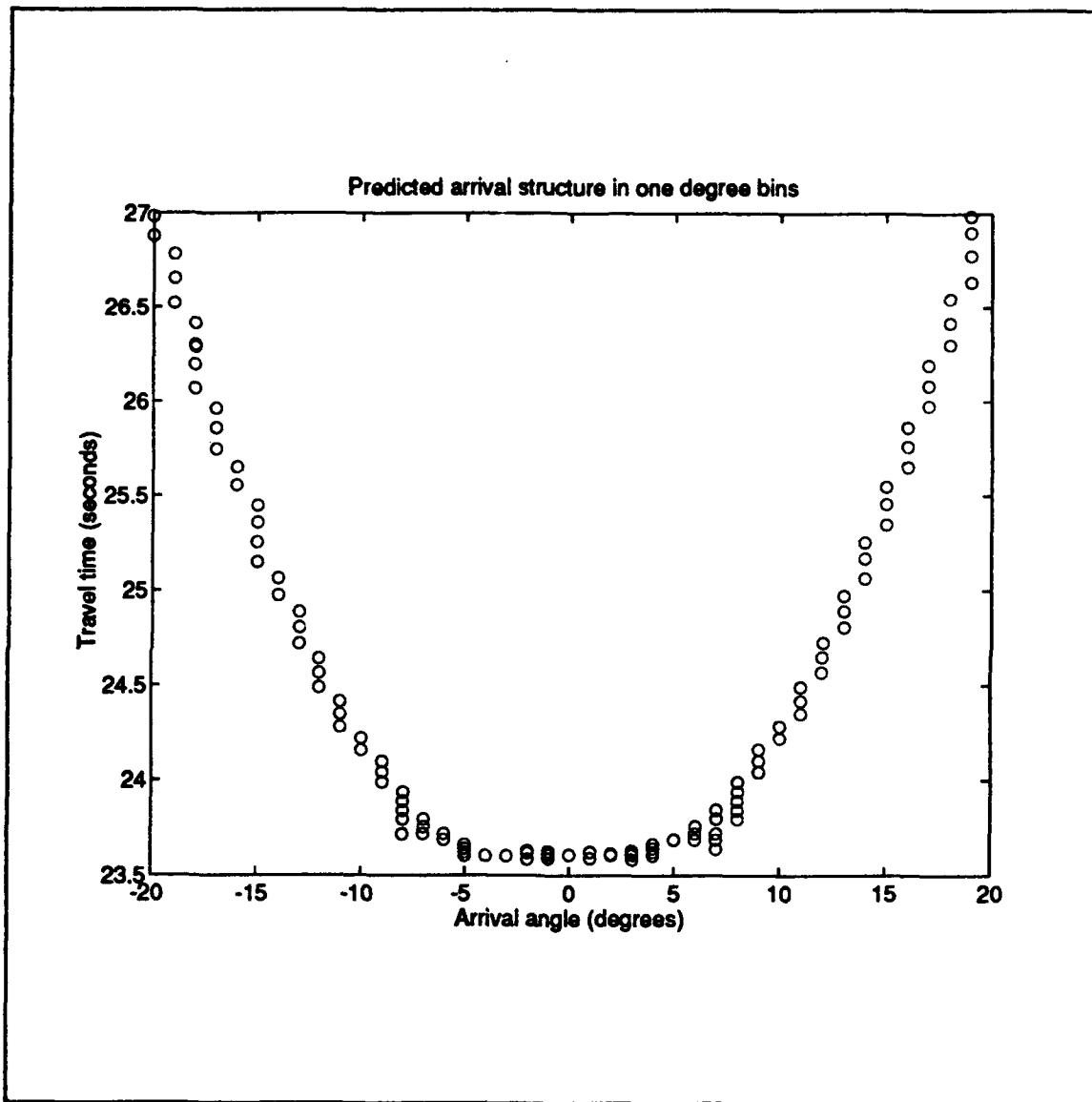


Figure 4.5: Predicted plane arrival structure in one degree bins.

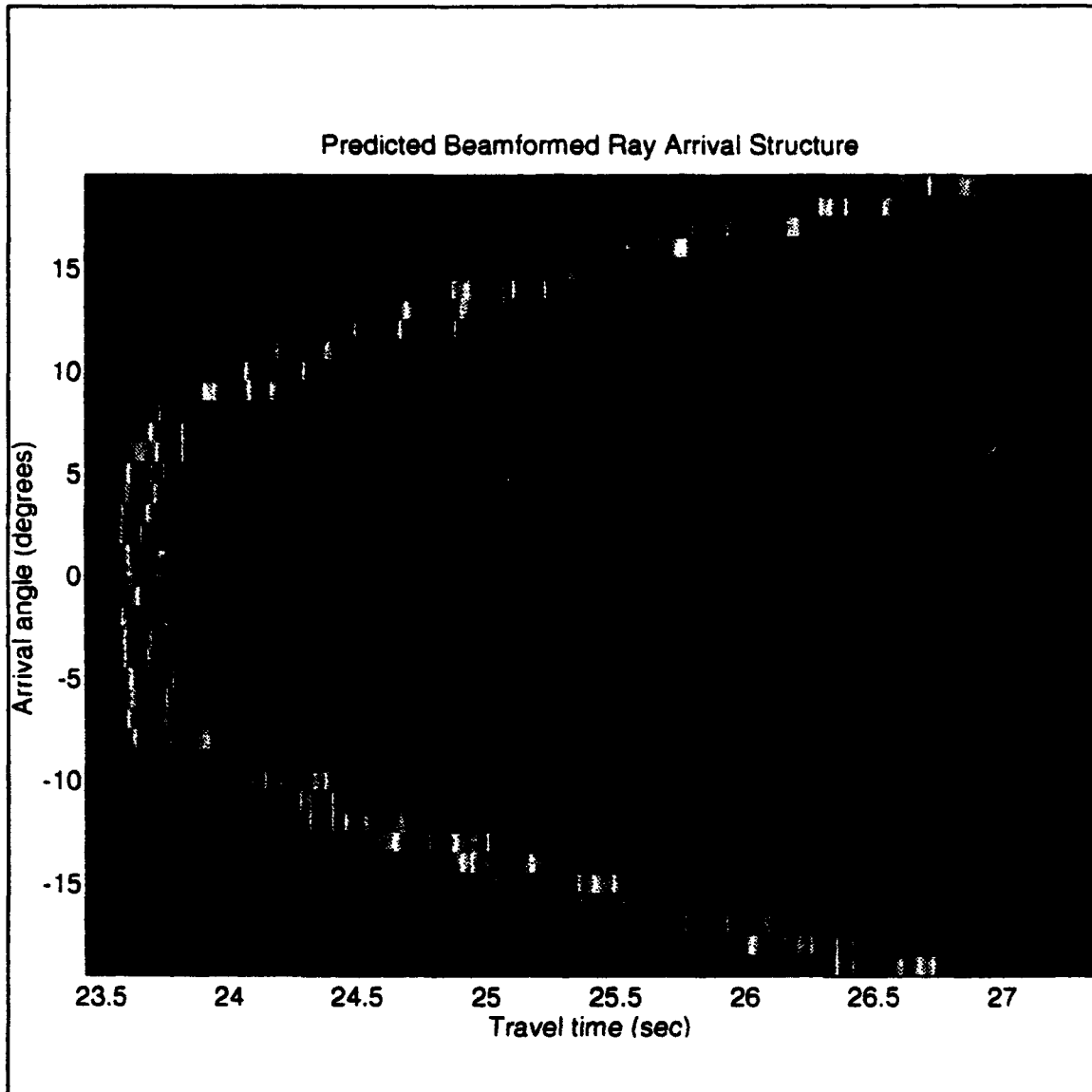


Figure 4.6: Predicted plane wave beamformed arrival structure [Ref. 3].

B. MODAL BEAMFORMER PREDICTIONS

Modal beamformer performance prediction is more difficult. The modal beamformer depends upon using a spatial filter to discriminate modes. The weights for the spatial filter depend upon knowing the mode shapes. Mode shapes at the array are dependent upon the sound speed profile and the boundary conditions. Performance will depend upon how well the environment is known at the array and how much the environment changes.

The modal beamformer is described by Equation 3.21. The performance of the beamformer depends upon the modes being orthogonal as described in Equation 3.10. A measure of the cross talk at a given frequency can be determined by approximating Equation 3.10 over the extent of the array aperture as:

$$r_{n,m} = \frac{\Delta z}{\rho_o} \sum_{k=0}^{15} Z_n(k) Z_m(k) \quad (4.1)$$

where k is the hydrophone depth, n and m are mode numbers, and the result is interpreted as the fraction of energy from mode n when beamforming for mode m . Ideally the result would be zero unless $n=m$ in which case the result would be one. Using Equation 4.1 at the center frequency of 224 Hz, Figure 4.7 was generated. This figure shows that modes one through three are well resolved. Modes one through three all having turning depths within the array so are expected to perform well [Ref. 9]. For higher modes, crosstalk is expected.

As with the plane wave beamformer, temporal separation of the modes also will assist in identification. Figure 4.8 shows the expected modal arrival structure. Figure

4.9 shows the ideal modal beamformed expected arrival structure. Figure 4.9 would be achieved if the vertical line array covered the entire water column. Figure 4.10 shows the effect of the beamformer. Comparing Figure 4.9 and Figure 4.10 we see the arrivals are visible and the timing remains intact but the cross talk is evident with more than one arrival visible.

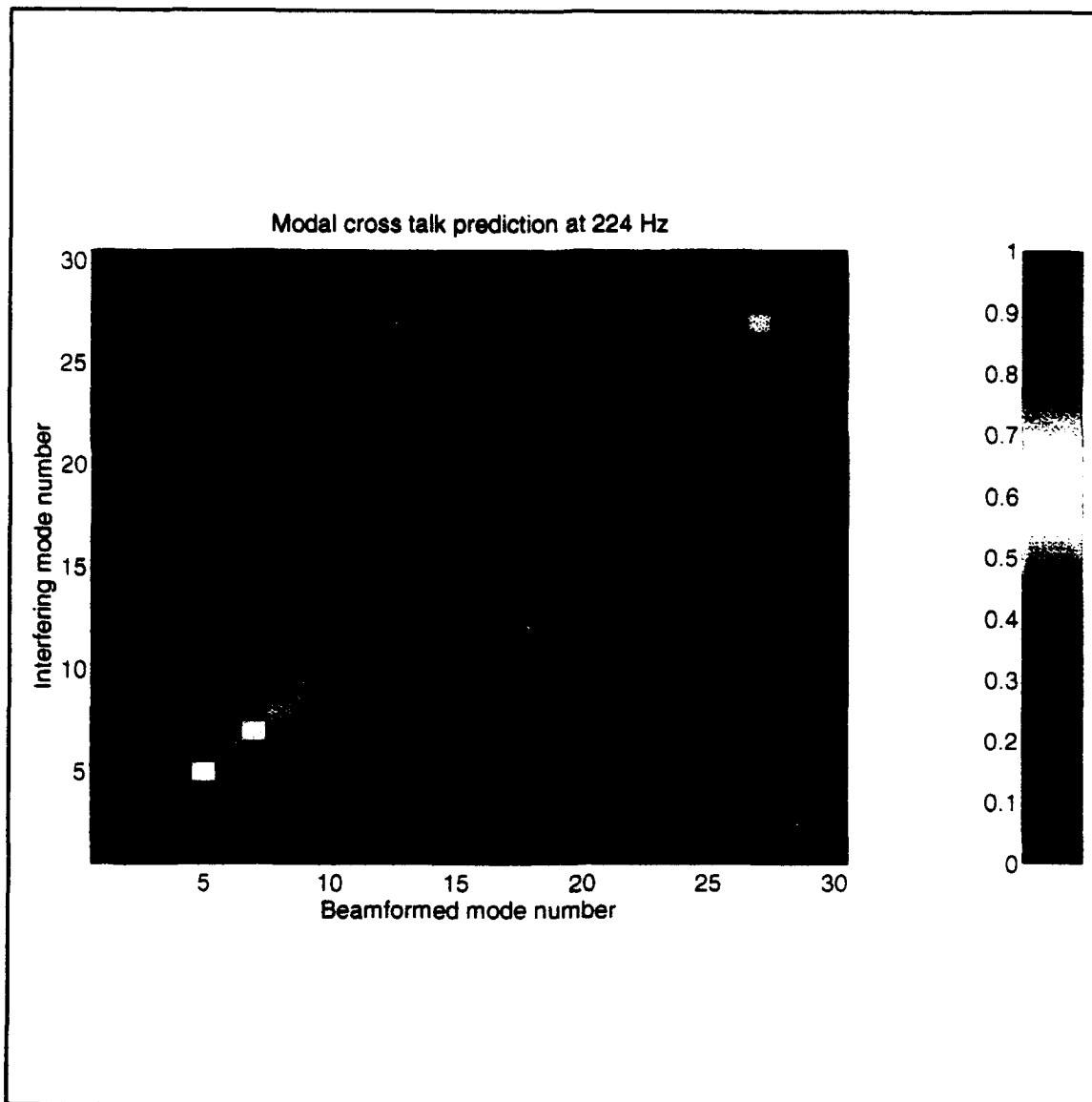


Figure 4.7: Predicted modal beamformer crosstalk.

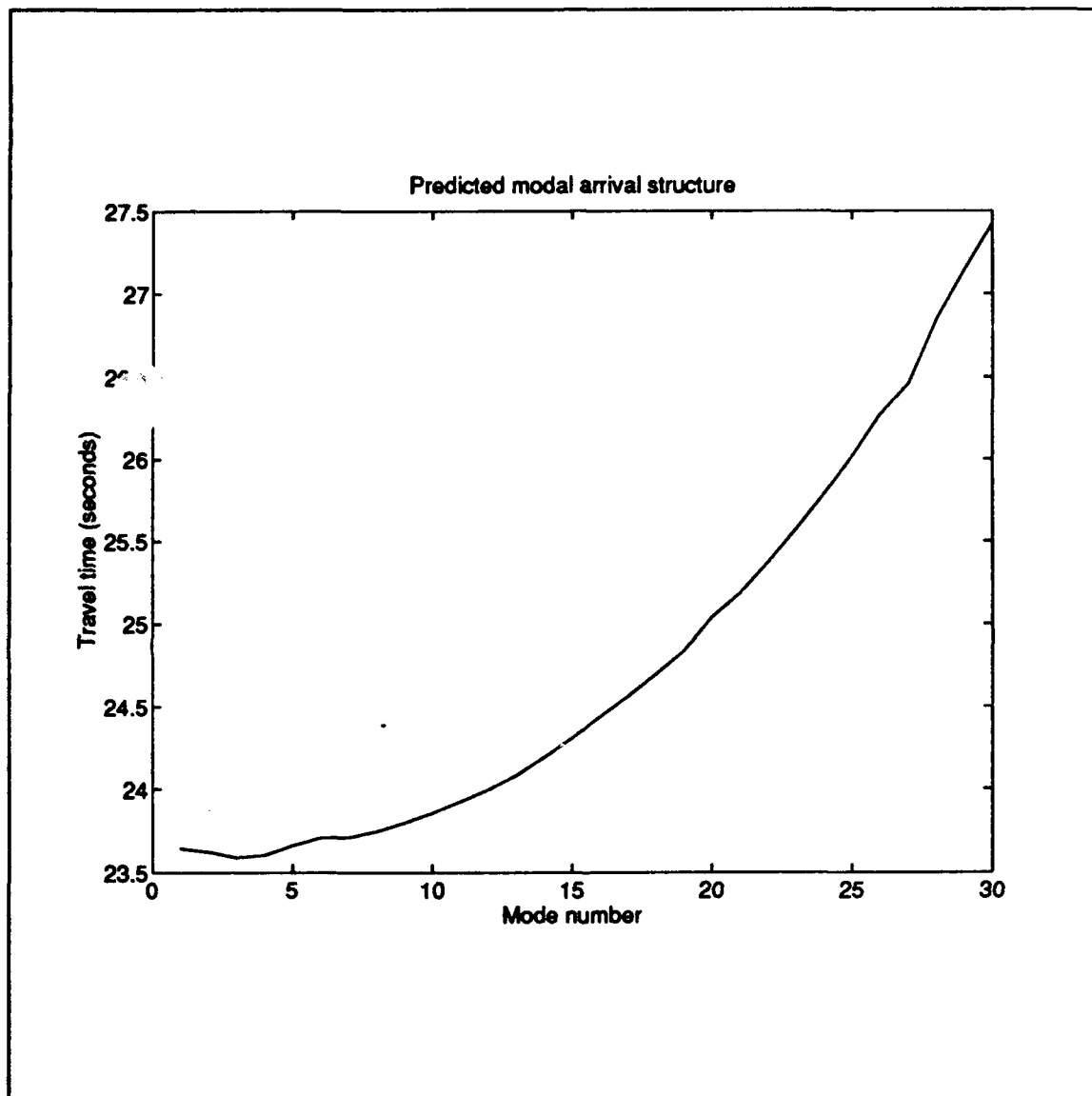


Figure 4.8: Predicted modal arrival structure [Ref 3].

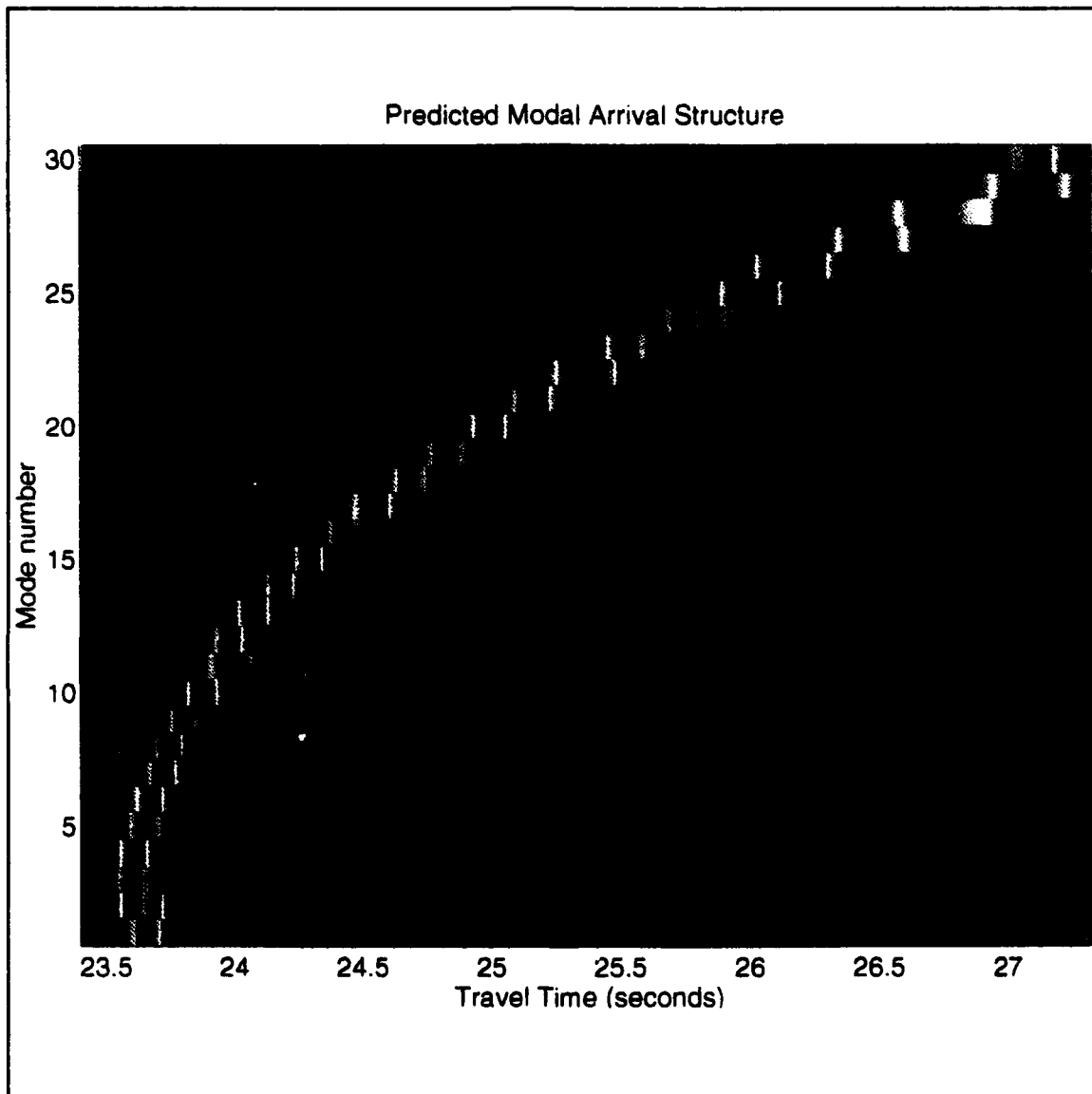


Figure 4.9: Ideal modal arrival structure. The "perfect" beamformer would have no cross talk [Ref 3].

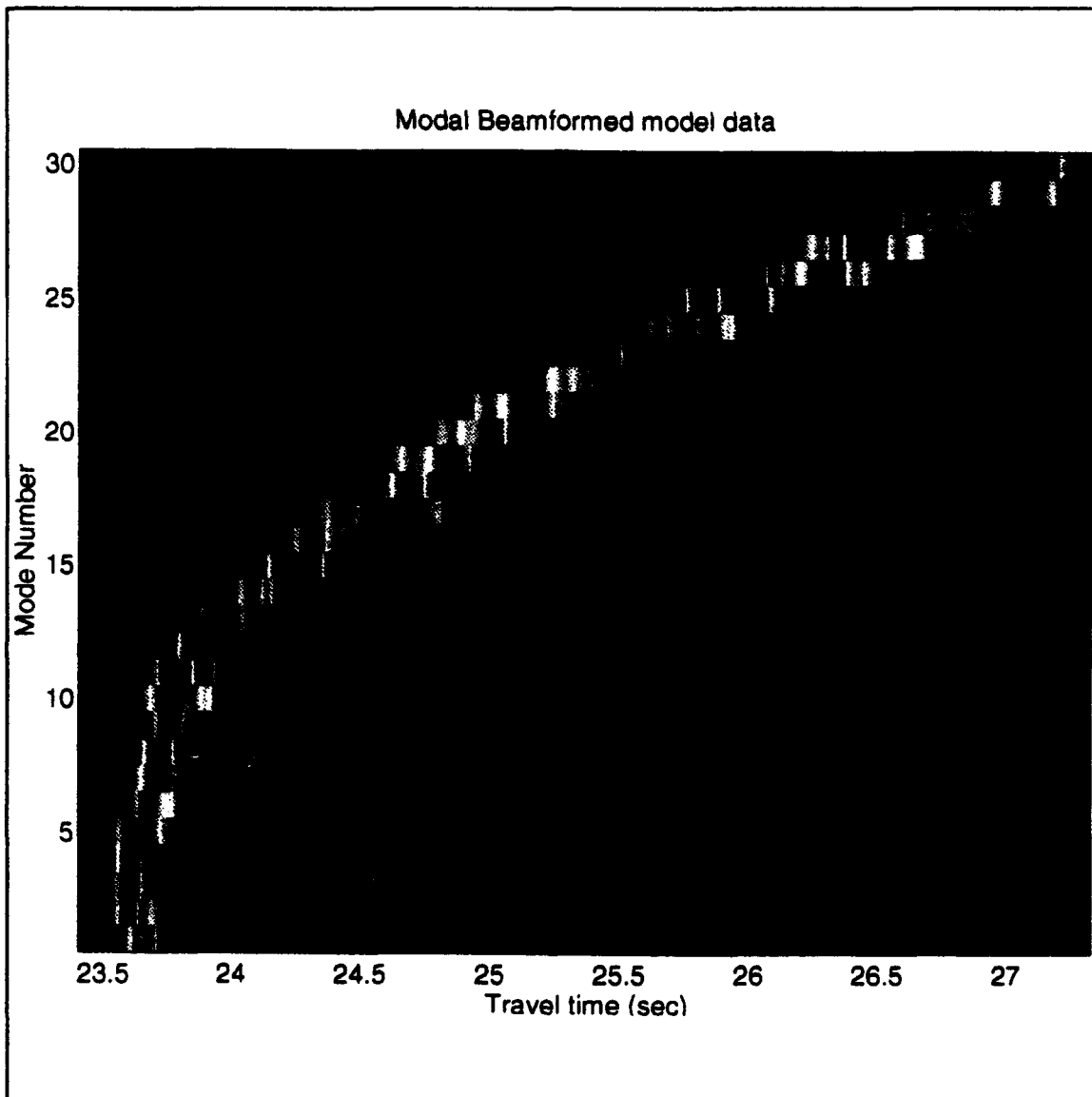


Figure 4.10: Beamformed synthetic data. This figure shows the expected cross talk between modes. Temporal separation makes arrival identification possible [Ref. 3].

V. RESULTS

A. PLANE WAVE

Plane wave beamforming was performed on 13 hours 20 minutes of acoustic data. For each five minutes of data, there were 30 transmissions of 3.9375 seconds. Of these 30 transmissions, the middle 28 were analyzed. The first and last transmissions were not used because the pulse compression of the signal was done in the frequency domain thus requiring a periodic signal. Using circular convolution, the first and last sequence may not have acoustic data over the time analyzed. After beamforming each of the 28 seconds of data from -19 to +18 degrees, the 28 sequences were coherently averaged prior to peak detection, identification, and tracking.

Figure 5.1 shows a sample of decoded signals on hydrophone seven for one set of 30 transmissions. Only the middle 28 arrivals are shown. The arrivals show a large peak in the beginning which is from low angle arrivals. Beamforming is necessary to distinguish different individual arrivals in the initial large peak and to bring out later arrivals. After beamforming, the 28 arrivals are coherently averaged. This figure shows the consistency in the signal over the different transmissions.

Figure 5.2 shows an example of plane wave beamformed output. The figure is windowed for a region of time which the arrivals are expected. The actual arrivals are indicated by the red regions. Note that multiple arrivals are apparent as was predicted in the forward model. It is the difference between the arrivals shown in Figure 5.2 and

Figure 4.6 which provide the information for the inverse algorithm. Figure 5.3 shows an example of actual detected peaks and modeled peaks. Using information as shown in Figure 4.3, sound speed maps were produced for each five minutes [Ref. 3]. An example of a sound speed map is shown in Figure 5.4.

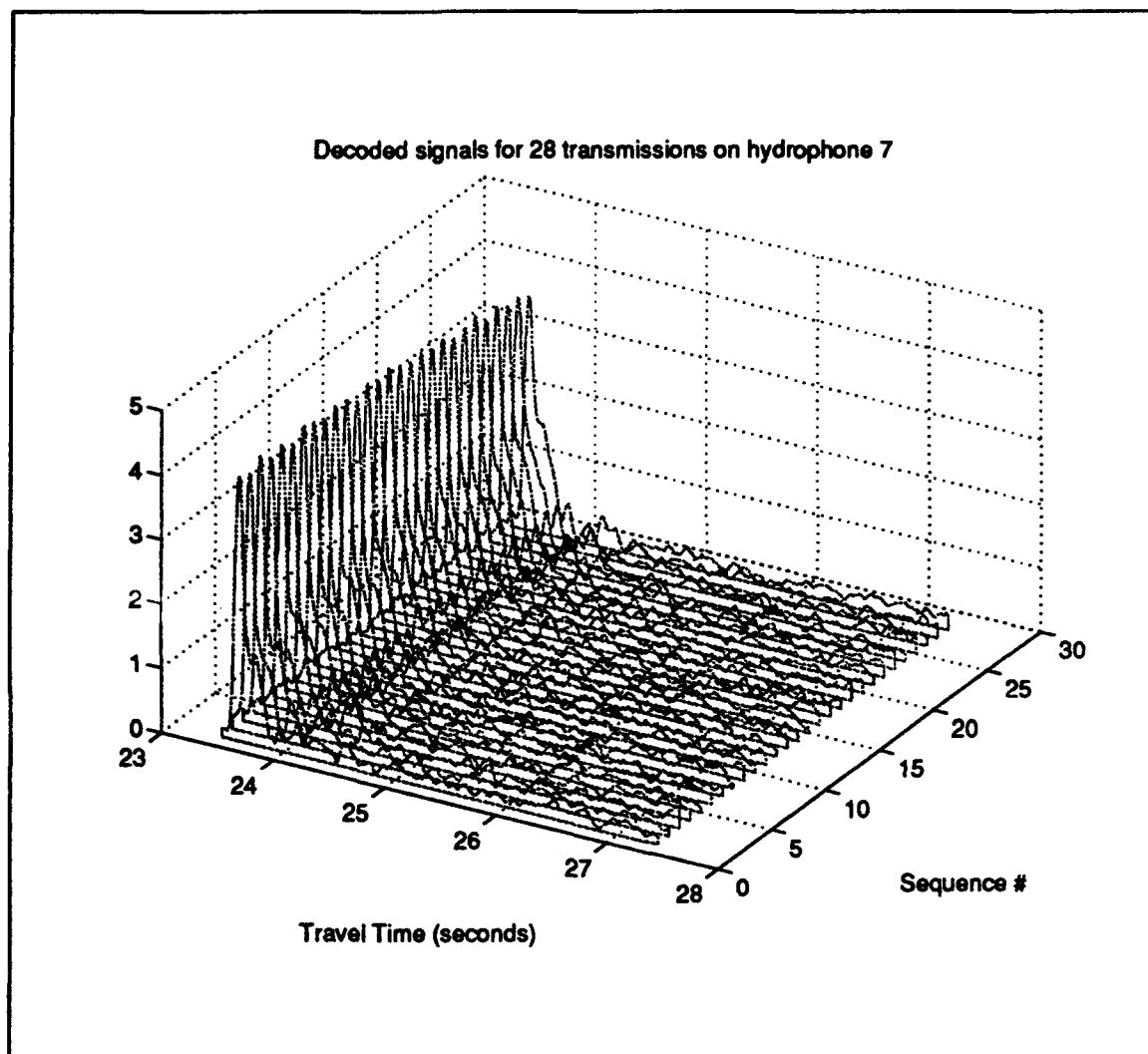


Figure 5.1: Example of decoded acoustic signal.

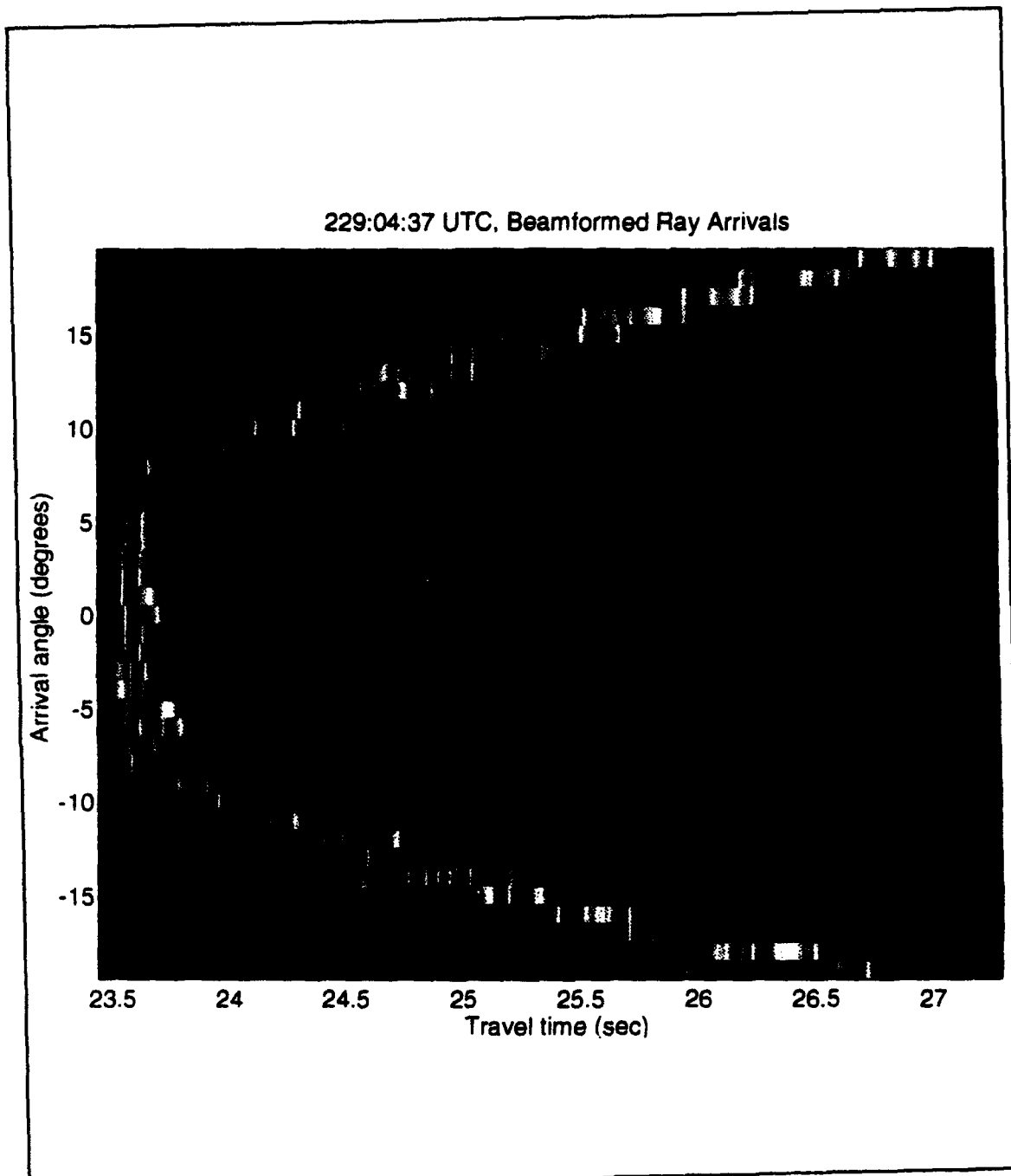


Figure 5.2: Example of plane wave beamformed output.

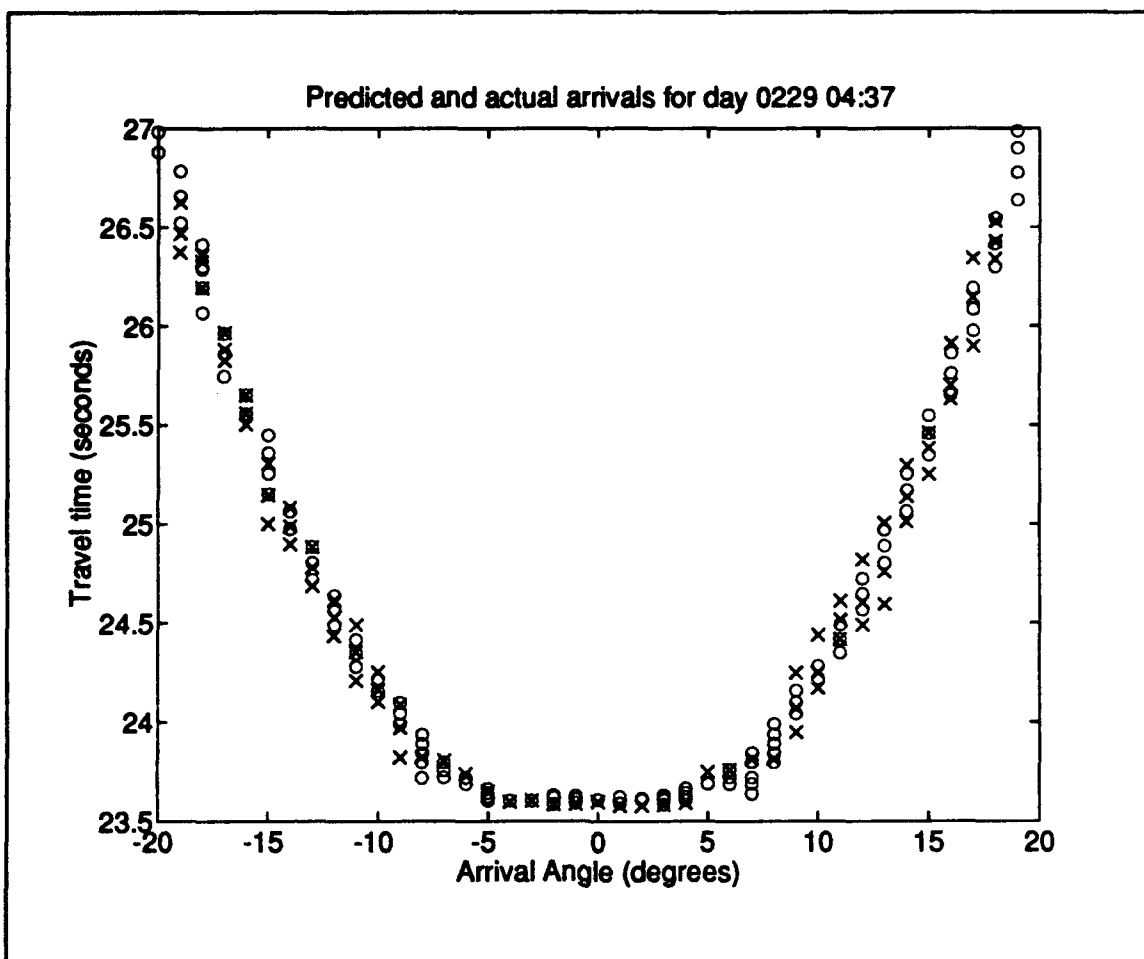


Figure 5.3: Example of model predicted arrival times with detected arrival times for plane wave beamformer. Predicted 'o', actual 'x'. Predictions as in Ref. 15.

Figure 5.4 clearly shows the Barents Sea Polar Front. The Front has a fine vertical structure. The warm and salty Atlantic water is to the south and is indicated on the map by the red and yellow regions. From the processed acoustic data, 160 frames were produced similar to Figure 5.4 [Ref. 3]. These frames were then transferred to video tape producing a movie of the frontal dynamics over the tidal period. A summary of the data used to produce this video is show in Figure 5.5.

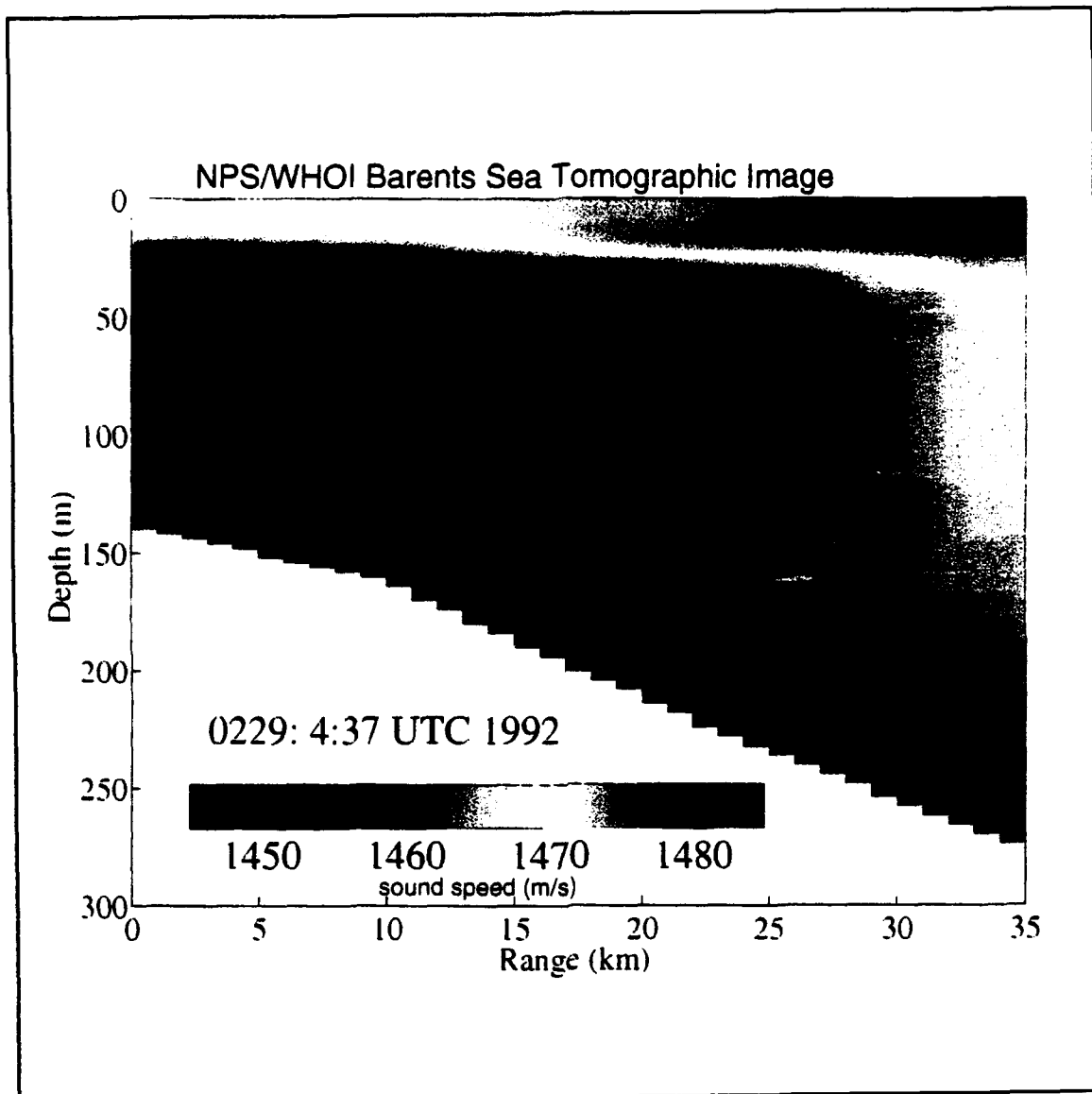


Figure 5.4: Example of sound speed map generated by the inverse algorithm developed by Chiu [Ref. 3].

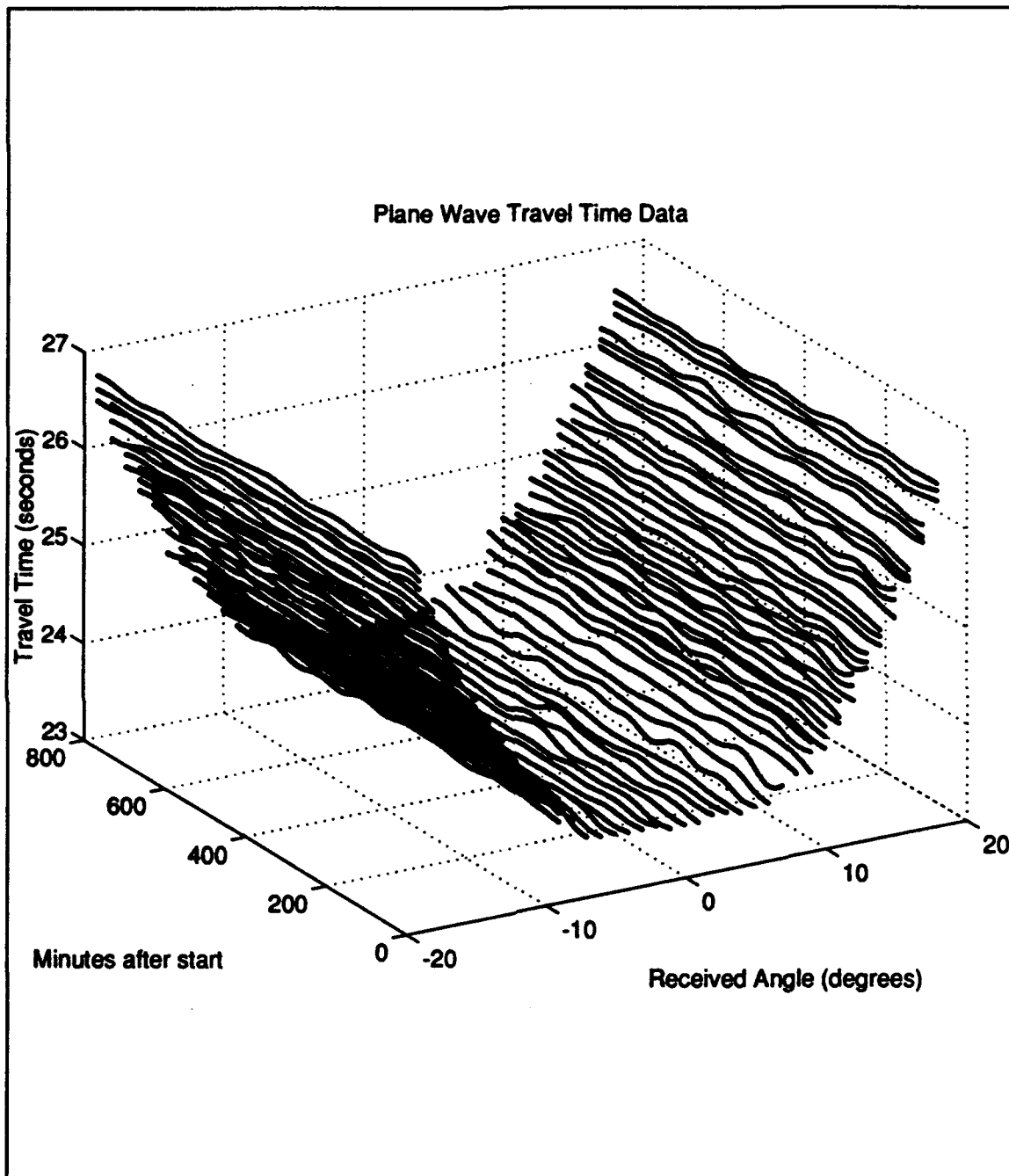


Figure 5.5: Summary of travel time data determined through plane wave beamforming. This data was used to produce a sound speed movie.

Wavefront correction was attempted for the plane wave beamforming but no significant improvement was noted. The wavefront correction was determined using model wavefront curvature for the background sound speed field [Ref 6]. The model prediction for the wavefront curvature are difficult because of some limitations of the model. Small local variations in the bathymetry results in arrivals which are not smooth. This is because HARPO treats the rays as having no radius [Ref. 14]. Thus the rays do not ensonify a region of the bottom but instead reflect off a point and are not influenced by the region.

B. MODAL BEAMFORMING RESULTS

Modal beamforming was performed on the 13 hours and 20 minutes of data. Two types of beamforming was done. The first modal beamforming was an outer product performed as indicated in Equation 3.29 with its associated beampattern shown in Figure 4.7. This beamforming yielded identifiable arrivals. Figure 5.6 shows an example of modal beamformed output. Note the similarities between Figures 5.6 and 4.9. The arrivals can be identified as the red regions near the center of the windows. Windowed regions are shown to make arrivals easier to identify. Evidence of the crosstalk between modes can be seen in both Figures 4.9 and 5.6. Figure 5.7 shows an example model predicted arrival times and beamformed arrival times. The difference between these is the information that can be used for the inverse algorithm to determine spatial sound field. A summary of travel modal travel time results is shown in Figure 5.8.

A least-squares approach was also used for modal beamforming. Using Equation 3.46 weights were determined using least-squares for the first 14 modes. Higher modes were not analyzed because the solution became ill conditioned for more than 14 modes. While this method produced results which were consistent, the outer product beamformer produced results which could be used to identify and track arrivals for 30 modes.

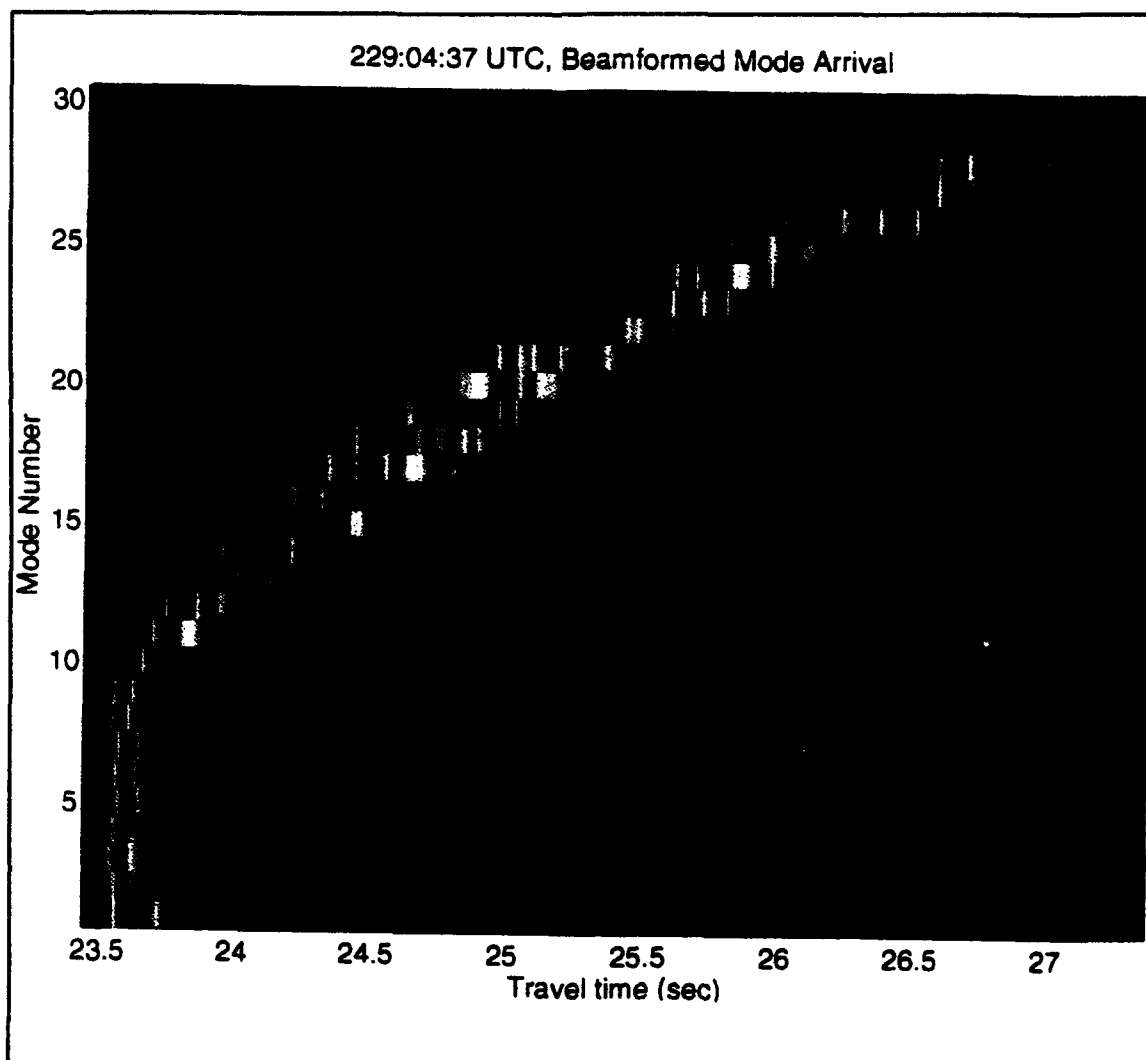


Figure 5.6: Example of modal beamformed output.

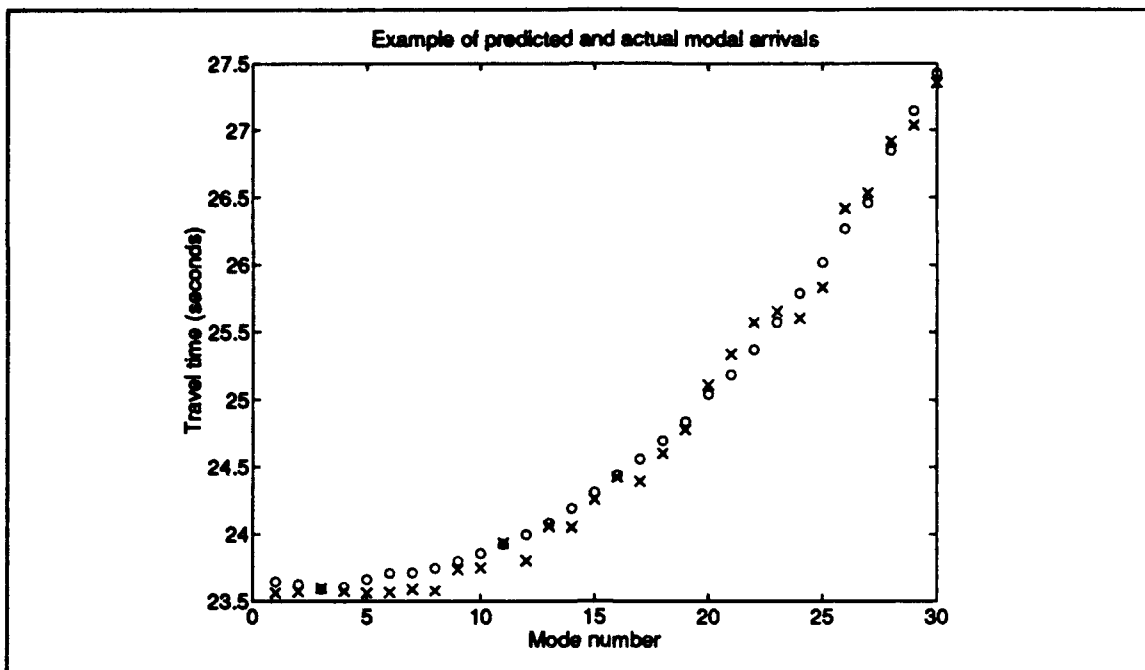


Figure 5.7: Example of modal travel time prediction and actual detected travel times. Model predictions indicated by 'o', actual travel time indicated by 'x'. Predictions from [Ref. 3].

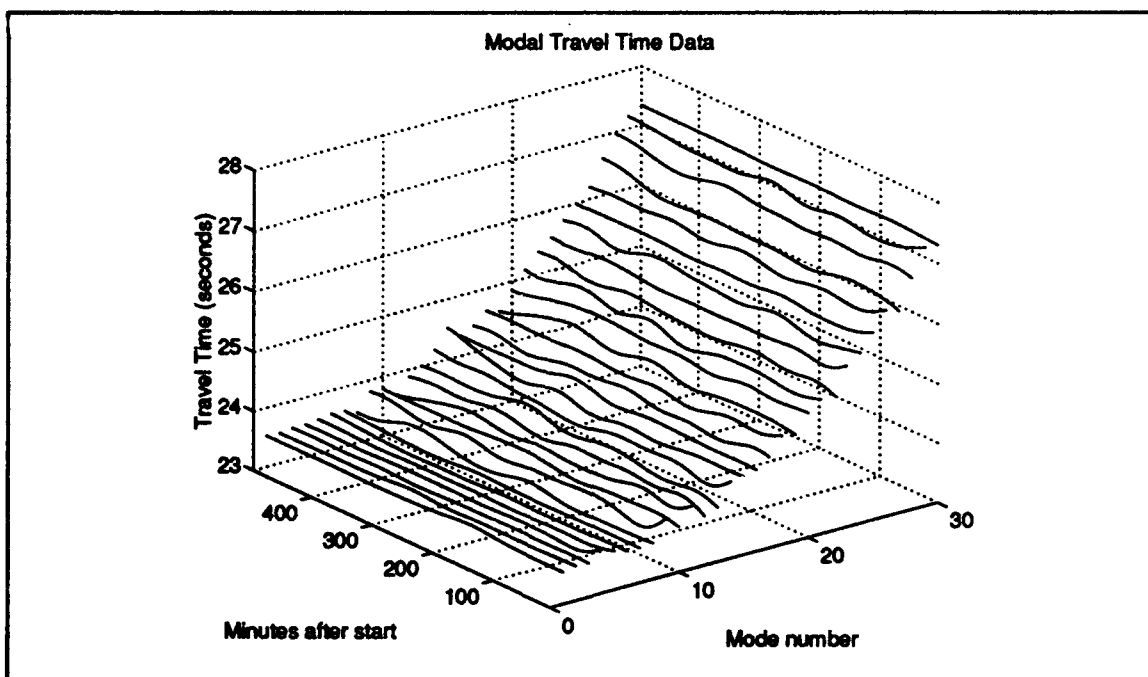


Figure 5.8: Summary of modal arrival travel times. This data can be inverted to produce sound speed maps.

VI. SUMMARY AND FUTURE WORK

A. SIGNAL PROCESSING SUMMARY

Temporal and spatial signal processing algorithms were developed and applied to acoustic data acquired in the Barents Sea Polar Front Experiment in 1992. Over 13 hours of acoustic data was processed for plane waves without wavefront corrections and over eight hours was processed for normal modes. An arrival detection, identification, and tracking algorithm was developed and applied to both modal and plane wave beamformed data. Results without wavefront correction were predicted to be adequate to resolve arrivals. The output of the plane wave beamformer without wavefront correction yielded adequate results to develop tomographic images.

Wavefront correction was attempted but while the ray model produced accurate results for arrival estimation, model limitations prevented accurate wavefront information. Tracing rays at finer launch angles may yield sufficient data to perform wavefront correction. With more data smoothing could be done to produce reasonable wavefront corrections. There are indications of a great deal of variability in the sound speed map. The background model may not provide accurate enough predictions over a long period of time to correct for wavefront curvature.

Modal beamforming was conducted using a dot-product and least-squares approach. The dot-product beamformer produced adequate results to determine arrival information for 30 modes. These results should be adequate for future inversion. The least-squares

beamformer was limited to the first 14 modes because the solution became ill conditioned for more. An array with more elements should allow a least-squares solution for more modes. The least-squares approach should produce a more statistically reliable beamformer but more array elements are needed for a better solution.

B. FUTURE WORK

The algorithms are complete for plane wave and modal beamforming. The data which was processed was chosen because it was the largest continuous block of time. There are other blocks of time which could be processed. After completion of processing a linear interpolation could be done to extend the period of time covered by the movie.

Wavefront correction should be analyzed further. The first cut would be to perform ray tracing using HARPO with smaller differences in launch angle, beginning with 0.001 degrees between launch angles. *Then analyze the data for improvement.* A second cut would be to perform ray tracing using the sound speed maps which have been previously generated. These sound speed fields should produce more accurate ray tracing results.

Perform a detailed study on least-squares beamformer performance. Begin with synthetic data with a known noise field added. Then determine if the least-squares beamformer produces better results as measured by travel time error estimation.

The beamformer code is currently written to be able to run on computers with relatively small amounts of RAM. With access to better computers, the beamformer code can be optimized to run much faster. Program speed was limited by read/writes to hard

disks for temporary storage. Eliminating unnecessary disk writes should speed the execution time of the program significantly.

C. RECOMMENDATIONS

The greatest impact on modal beamforming performance is the sound channel coverage. A longer array with more elements would improve the modal beamformer. The modal beamformer also depends upon accurately knowing the mode shape at the hydrophones. This requires knowing where the hydrophones are in depth. Tilt information was available for the array and a linear tilt model was used. The vertical array likely has curvature from currents and tilt. Better array shape information would improve processing through accurate knowledge of hydrophone position.

REFERENCES

1. S. O'Keefe, "...From the Sea: preparing the naval service for the 21st century: a new direction for the naval service," U. S. Navy, 1992.
2. W. Munk and C. Wunsch, "Ocean Acoustic Tomography: A Scheme for Large Scale Monitoring," *Deep-Sea Research*, v. 26A pp. 123-161, 1979.
3. C.-S. Chiu, J. H. Miller, J. F. Lynch, "Inverse Techniques for Coastal Acoustic Tomography," Accepted for the Proceedings of the 1993 International Conference on Theoretical and Computational Acoustics, July 1993.
4. J. H. Miller, C.-S. Chiu, J. F. Lynch, "Signal Processing for Coastal Acoustic Tomography," Accepted for the Proceedings of the 1993 International Conference on Theoretical and Computational Acoustics.
5. R. Bourke, C.-S. Chiu, J. Lynch, J. Miller, R. Muench, A. Plueddemann, "Preliminary Cruise Results: Barents Sea Polar Front Experiment," Barents Sea Polar Front Group, unpublished, August 1992.
6. J. Mykyta, *Prediction of the Plane Wave Beamformed Acoustic Arrival Structure for the 1992 Barents Sea Coastal Tomography Test*, MS Thesis, Naval Postgraduate School, Monterey, CA, September 1993.
7. J. M. Emblidge, *A Feasibility Study of Ocean Acoustic Tomography In The Barents Sea*, MS Thesis, Naval Postgraduate School, Monterey, CA, September 1991.
8. H. Loeng, *Features of the Physical Oceanographic Conditions of the Barents Sea*, unpublished manuscript, 1991.
9. G. A. Omans, *Broadband Modal Beamforming of Acoustic Tomography Signals Acquired By A Vertical Array*, MS Thesis, Naval Postgraduate School, Monterey, CA, September 1992.
10. R. C. Dees, *Signal Processing and Preliminary Results in the 1988 Monterey Bay Tomography Experiment*, MS Thesis, Naval Postgraduate School, Monterey, CA, June 1989.

11. K. von der Heydt, J. Kemp, J. Lynch, J. Miller, and C.-S. Chiu, "Array Data Acquisition with Wireless LAN Telemetry as applied to Shallow Water Tomography in the Barents Sea," Technical Report WHOI-92-44, Woods Hole Oceanographic Institution, Woods Hole, MA, December 1992.
12. R. C. Spindel, "Signal Processing in Ocean Tomography," *Adaptive Methods in Underwater Acoustics*, ed. H.G. Urban, pp. 687-710, D. Reidel Publishing Company, 1985.
13. L. E. Kinsler and others, *Fundamentals of Acoustics*, 3rd edition, John Wiley & Sons, 1982.
14. R. M. Jones, J.P. Riley, and T.M. Georges, *HARPO: A versatile three-dimensional Hamiltonian ray-tracing program for acoustic waves in an ocean with an irregular bottom*, Wave Propagation Laboratory, NOAA, Boulder, Colorado, 457 pp., 1986.
15. E. C. Shang, "Ocean acoustic tomography based on adiabatic mode theory," *J. Acoust. Soc. Am.*, 85 (4), pp. 1531-1537, 1989.
16. R. Ziemer and R. Peterson, *Digital Communications and Spread Spectrum Systems*, Macmillan Publishing Company, 1985.
17. T. G. Birdsall and K. Metzger, "Factor Inverse Matched Filtering," *J. Acoust. Soc Am*, 79(1), 91-99 (1986).
18. P. B. Liebelt, *An Introduction to Optimal Estimation*, Addison-Wesley Publishing Company, 1967.

INITIAL DISTRIBUTION LIST

	No. Copies
1. Defense Technical Information Center Cameron Station Alexandria VA 22304-6145	2
2. Library, Code 52 Naval Postgraduate School Monterey CA 93943-5002	2
3. Department Chairman, Code EC Department of Electrical and Computer Engineering Naval Postgraduate School Monerey, CA 93943	1
4. Prof. J. H. Miller, Code EC/Mr Department of Electrical and Computer Engineering Naval Postgraduate School Monterey, CA 93943	5
5. Prof. C. S. Chiu, Code OC/Ci Department of Oceanography Naval Postgraduate School Monterey, CA 93943	1
6. Prof. R. Bourke, Code OC/Bk Department of Oceanography Naval Postgraduate School Monterey, CA 93943	1
7. Dr. J. F. Lynch Woods Hole Oceanographic Institution Woods Hole, MA 02543	1
8. Mr. K. Von der Heydt Woods Hole Oceanographic Institution Woods Hole, MA 02543	1

- | | | |
|-----|---|---|
| 9. | Dr. W. Jobst
NAVOCEANO
Code 0
Stennis Space Center, MS 39522 | 1 |
| 10. | LT P. G. McLaughlin, USN
2419 E. Fairfield
Mesa, AZ 85213 | 1 |
| 11. | Dr. R. C. Spindel
Director, Applied Physics Laboratory
University of Washington
1013 Northeast 40th Street
Seattle, WA 98105 | 1 |
| 12. | Prof. T. Birdsall
Communications and Signal Processing Laboratory
Department of Electrical Engineering and Computer Science
University of Michigan
Ann Arbor, MI 48109-2122 | 1 |
| 13. | Dr. Kurt Metzger, Jr.
Communications and Signal Processing Laboratory
Department of Electrical Engineering and Computer Science
North Campus
University of Michigan
Ann Arbor, MI 48109-2122 | 1 |
| 14. | Prof. A. B. Baggeroer
Department of Ocean Engineering
Massachusetts Institute of Technology
Cambridge, MA 02139 | 1 |
| 15. | Dr. T. Curtin
Office of Naval Research
800 North Quincy Street
Arlington, VA 22217-5000 | 1 |
| 16. | Dr. M. Badiy
Office of Naval Research
800 North Quincy Street
Arlington, VA 22217-5000 | 1 |